OBSERVED EXTREME RAINFALL TRENDS ALONG THE UNITED STATES GULF AND SOUTHEASTERN COASTS

A Thesis

by

SAVANNAH K. JORGENSEN

Submitted to the Graduate and Professional School of
Texas A&M University
in partial fulfillment of the requirements for the degree of

MASTER OF SCIENCE

Chair of Committee,	John Nielsen-Gammon
Committee Members,	Yangyang Xu
	Mikyoung Jun
Head of Department,	Ramalingam Saravanan

May 2022

Major Subject: Atmospheric Sciences

ABSTRACT

Rainfall that occurs at the tails of the precipitation distribution are considered to be the extremes, which are of critical importance for regional flood planning and infrastructure design. Previously, a stationary climate assumption had been used for computing extreme rainfall estimates. However, this assumption has since been shown to underestimate current precipitation frequency and intensity in the presence of an upward trend in precipitation. Trends in the rainfall extremes, calculated through a nonstationary lens, have been documented in observations and global climate models. This study computes extreme rainfall trends across the Gulf and Southeastern Coasts of the US and presents additional methods for addressing current uncertainties in assessing the climate-driven trends. Nonstationary generalized extreme value (GEV) models are applied to historical data (1890-2019) and fit to the log of precipitation while using CMIP5 global mean model surface temperature as the covariate. Comparisons are also made to NOAA Atlas 14 using a stationary GEV model and truncated datasets.

Trends for the composite stations vary from -30% to ~ +60% across the area of study while the pooled trends vary from -5% to +27% at the 2-yr return period and -8% to ~ +50% at the 100-yr return period. The trend estimates themselves are sensitive to various weather events and are therefore unreliable as individual estimates. The aggregate of the pooled trends yield mean trend estimates and associated 95% confidence intervals of 8.99% +/- 3.90% for the 2-yr return period and 13.43% +/- 3.91% for the 100-yr return period using a spatial statistical model. Through the

comparisons to NOAA Atlas 14 extreme rainfall estimates, it can be seen that updates to the stationary estimates are necessary.

ACKNOWLEDGEMENTS

I first would like to thank my advisor, Dr. Nielsen-Gammon for his support and mentorship throughout my master's education. I have been challenged to think more critically and grow as a scientist each step of the way because of his guidance. I would also like to thank my committee members, Dr. Xu and Dr. Jun, for their support throughout this process. Thank you to Dr. Jun and her PhD student, Lingling Chen, for assisting me with the spatial statistics in this research and for providing me with the R script that I used to perform such statistics.

Of course, any acknowledgements would not be complete without thanking my family and friends. To my family, thank you for always being there for me as I continue to pursue higher levels of education. While you may not always understand the work that I am doing, you certainly are excited whenever I talk about it, and for that, I am so grateful. Thank you to my inner circle of friends from undergrad. You know who you are. We've been through a lot together, including grad school now. I couldn't have gotten here without your constant support and friendship.

Lastly, I want to thank all my friends that I've made in grad school, including but by no means limited to my research group (Alex, Alexa, and Judy), Leland, Justin, and Sydney. You all have gotten me through the ups and downs of this master's degree. Thank you from the bottom of my heart.

CONTRIBUTORS AND FUNDING SOURCES

Contributors

This work was supervised by a thesis committee consisting of Professor John Nielsen-Gammon and Professor Yangyang Xu of the Department of Atmospheric Sciences and Adjunct Professor Mikyoung Jun of the Department of Statistics.

The R script that analyzed the gaussian process model for Section 2 was provided by Lingling Chen. All other work conducted for the thesis was completed by the student independently.

Funding Sources

Graduate study was supported by the Office of the State Climatologist (Texas A&M University) and the Harris County Flood Control District.

TABLE OF CONTENTS

Page

LIST OF FIGURES

Page

LIST OF TABLES

Page

1. INTRODUCTION

1.1. Background

Future extreme precipitation, such as the greatest one-day rainfall in a decade at a given location, has been examined under different statistical lenses within existing literature. Previous planning estimates have utilized the stationary climate assumption in extreme precipitation calculations (Hershfield 1961; Bonnin et al. 2006; Perica et al. 2013; Perica et al. 2018). Nonstationarity, as seen by trends in data, has been increasingly shown to be an important consideration for extreme precipitation analysis (Kunkel et al. 2013; Westra et al. 2014; Pacoriek et al. 2018). The stationary assumption can underestimate the present-day frequency and intensity of extreme precipitation events in the presence of an upward trend in precipitation and recent heavier rain-producing storms (Wright et al. 2019; Vu and Mishra 2019).

In the context of a warming climate, precipitation has a potential to increase as the result of an enhanced atmospheric capacity for holding water vapor, according to the Clausius-Clapeyron relationship. The relationship predicts a ~7% increase in saturation vapor pressure per degree Kelvin increase in temperature (Held and Soden 2006; Westra et al. 2014). However, changes in weather patterns and storm structure can also affect precipitation intensity (Trenberth 2011; Prein et al. 2017).

Before observed changes in precipitation began to be documented, rudimentary models were already showing that extreme rainfall would likely increase in the future (Fischer and Knutti 2016). More sophisticated models and ensembles, such as the

Coupled Model Intercomparison Project Phase 5 (CMIP5), have broadly been supporting this pattern as well (Knutti and Sedlacek 2012; Pfahl et al. 2017; Giorgi et al. 2019; Feng et al. 2019). Globally, modeling studies have shown extreme rainfall increasing in North America, Europe, South Africa, and Oceania, and decreasing extreme rainfall in Eastern China, with more variability in the trends at smaller spatial scales (Westra et al. 2014). Mascioli et al. (2016) examined the US in their modeling study, which found increasing trends in wintertime extreme precipitation over the eastern US for simulations that considered greenhouse gas forcing only. Simulated springtime extreme precipitation increased over much of the central and eastern US (Mascioli et al. 2016). Other modeling works have also investigated trends in precipitation extremes in the US. For example, Janssen et al. (2014) showed that the frequency of extreme precipitation event days had a positive trend in the CMIP5 model simulations.

Some modeling studies have additionally made the distinction between simulations of the annual mean precipitation and the tails of the precipitation distribution, and in doing so, have demonstrated that rainfall is tending to shift toward the upper tails of the probability distribution function. This indicates that extreme precipitation is changing more than the annual mean (Pendergrass and Hartmann 2014; Giorgi et al. 2019).

Models also provide an overview of extreme precipitation behavior under a continually changing climate. Feng et al. (2019) used an ECMWF model to identify how light, moderate, and heavy precipitation frequencies would change as the global

temperature increased. The intensity of precipitation events in all precipitation categories increased at high latitudes, while the light and heavy precipitation frequencies increased (the PDF flattened as the frequencies spread out at the tails of the distribution) at the expense of moderate precipitation in the tropics under these simulations (Feng et al. 2019). Over most land regions in the subtropical and mid-to-high latitudes, the PDF reflected a shift toward higher frequencies of heavy precipitation events with a decrease in the moderate and light precipitation frequencies (Feng et al. 2019). Comparatively, Giorgi et al. (2019) highlighted that light and medium precipitation event frequencies would decrease while high precipitation event frequencies and intensities would increase under a 4 ℃ warming scenario over the majority of global land areas.

Precipitation simulation in models does continue to be filled with biases and uncertainties when compared to previous model iterations and observations. Typical biases include those related to seasonal mean precipitation and the number of days with precipitation (Dai 2006; Mehran et al. 2014). Model resolution in global climate models is also a factor in uncertainties. For example, light precipitation frequency tends to be overestimated while extreme precipitation frequency is usually underestimated in models due to the coarse resolution (van der Wiel et al. 2016). Trends in extreme precipitation amounts and frequency have also been underestimated by the CMIP5 models compared to observations (Janssen et al. 2014; Asadieh and Krakauer 2015). The CMIP6 models have been found to exhibit no significant differences from the CMIP5 models (Wehner et al. 2020a). Precipitation extremes are underestimated in the tropics but overestimated in the subtropics in CMIP6 models (Chao et al. 2021). However, CMIP6 models, like

previous CMIP iterations, do show an increase in frequency and intensity of extreme precipitation over much of the globe and capture the large-scale spatial patterns of extremes well (Chao et al. 2021). Janssen et al. (2014) found that the observations obtained from the US Cooperative Observer Network (COOP) stations also showed a positive trend in the frequency of extreme precipitation event days, which was a consistent finding in the CMIP5 model observations. However, the signal of the trends was reduced in the models.

Observational data is often used in more recent studies on extreme rainfall and can provide a means of verification for global model estimates while also contributing a higher resolution at which to analyze extreme precipitation patterns. On a global scale, the observed annual maximum daily precipitation has increased faster than in most CMIP5 climate models (Asadieh and Krakauer 2015). The increasing trend is broadly consistent on a continental scale as well, with documented increases in sub-daily and daily extreme precipitation noted across Europe, Asia, and North America (Westra et al. 2014; Sun et al. 2021). Other continents, such as South America and Africa, exhibit increases in extreme precipitation in areas that have good data coverage, although any trend calculations in those continents do contain uncertainties due to the sparsity of the data (Sun et al. 2021). Observations further support the conclusion from Pendergrass and Hartmann (2014) and Giorgi et al. (2019) that extreme precipitation is changing more than the annual mean. For example, Wu (2015) found that heavy precipitation increased at higher rates than the mean precipitation across the CONUS while looking at station

precipitation data; heavy precipitation increased at 4.24% per decade compared to 1.66% per decade for the annual trend (Wu 2015).

Studies for the US have shown a range of trend estimates at various levels of significance for different lengths of data records and aggregation magnitudes, with statistically significant trends found in durations from minutes to a few days (Kunkel et al. 2013; Westra 2014). On a regional scale, the Midwest, Northeast, and Southeast regions in the US have shown the largest upward trends in extreme precipitation (Kunkel et al. 2013).

Aggregated US trends in extreme precipitation are more likely to be statistically significant east of 100 °W (Wright et al. 2019; Kunkel et al. 2020). Wright et al. (2019) found this to be true in their study which used a regional aggregation approach for reducing the noise in extreme precipitation trends, which ultimately exhibited statistically significant increases in the frequency of exceedances for different return periods, with greater increases at longer return intervals. The aggregation in Kunkel et al. (2020) used the National Centers for Environmental Information climate regions. The largest positive trends in extreme rainfall were located in the Northeast, East North Central, and Central climate regions, with nearly all of the trends at each return period and duration statistically significant at the 0.05 significance level (Kunkel et al. 2020). A similar analysis of extreme precipitation trends across the US was conducted by Wu (2015). The same climate regions were used for the purposes of aggregation. While the period of record was shorter, Wu (2015) also showed an increase in heavy precipitation

for all climate regions except the West. Regions such as the Northwest and Southeast presented large increases in extreme precipitation events while the mean precipitation did not change significantly, further emphasizing what global models have been demonstrating regarding a shift in the precipitation distributions (Wu 2015).

While much of the previous extreme precipitation literature has concentrated on larger regional trend estimates, Villarini et al. (2013) and Brown et al. (2020) considered station level estimates to attempt to obtain the climate signal at a smaller spatial scale. The region of focus for Brown et al. (2020) was the Southeastern and Gulf Coasts of the US. Extreme hourly, rather than daily, precipitation data were acquired from weather stations in the NCEI Hourly Precipitation Database, and annual time series were created from that with supplemented records contributed by the Midwestern Regional Climate Center and the Iowa Mesonet. Only 6% of the station-level trends were found to be significant at the 0.05 significance level, while 6.4% were significant between the 0.05 and 0.10 level which combined to a total of ~12% of stations that had significant trends. Villarini et al. (2013) focused on a similarly sized area, the central US, which also included some states considered in the present work (Louisiana, Arkansas, Mississippi, and Alabama). However, daily precipitation totals were used again in this study rather than hourly data. Increasing trends of extreme precipitation were found in this study as well, with 93 out of the 447 stations considered, or 21% of stations, exhibiting a significant positive trend (Villarini et al. 2013). This is much larger than the amount of significant trends in Brown et al. (2020), however, there were many more stations used in Villarini et al. (2013), 447, compared to Brown et al. (2020), 50. These differences in

significant trends could also be a result of the different extreme precipitation durations between the two studies. This illustrates how variable extreme precipitation trend analysis can be, especially while using trend estimation techniques on non-aggregated station-level data.

Critically, natural variability in the climate system can impact the detection of the anthropogenic climate change signal within extreme precipitation analyses. Martel et al. (2018) investigated the role of natural variability on the detection of climate change trend signals for extreme precipitation and mean precipitation. Natural variability affected the annual 1-day extreme precipitation indices at the local scale more than the annual precipitation. It was also shown to influence the climate change signal into the mid-century at both the local and regional scales, while the climate change signal was more robust at the global scale (Martel et al. 2018). This highlights the importance of and complications surrounding the signal detection within extreme precipitation trend analyses.

Extreme precipitation risk is particularly relevant for the Gulf Coast and Southeastern regions of the US. Almost all of the top 100 largest area-averaged, multiday precipitation events for the period 1949-2018 occurred in the southeastern US (Kunkel and Champion 2019). Furthermore, the Gulf Coast and Southeastern regions of the US have some of the largest and most significant trends in extreme rainfall according to a range of aggregation methods and statistical tests (Kunkel et al. 2013; Wu 2015; Wright et al. 2019; Kunkel et al. 2020).

1.2. Research Goals and Hypotheses

It is important to acknowledge that trends in observed extreme precipitation are influenced by the length of the data record and the amount of spatial aggregation that is performed on the data. Different trend estimates can also occur as a result of trend calculation methods (e.g., linearly over time, such as with linear regression). Previous studies have focused on periods of record in the mid to late 1900s through present day rather than extending that period of record further back to create a longer data record for the purposes of trend analysis. A shorter period of record can lead to less robust trend results due to noise in the data and can lower the predictive power of a statistical model. In order to extend the data record back to 1890, this study utilizes a county composite station approach. These composite stations are then pooled in such a way that is distinct from other aggregation methods used in the literature presented here. The methodology behind the composite station creation and pooling techniques will be described in detail in the next section. Additionally, the present work approaches the GEV analysis differently than previous studies, which allows us to acquire information not otherwise present in those studies. Thus, the goal of the present work is to examine extreme precipitation across the Gulf and Southeast Coasts of the United States in order to expand upon existing extreme precipitation research and add additional methods that should help reduce current uncertainties in assessing the climate-driven trends. Our main hypotheses are:

1. Compositing and pooling techniques for station precipitation data will act as sound aggregation methods for analyzing extreme precipitation trends aside from other approaches used in the literature.

2. The extension of precipitation annual block maxima periods of record yields more robust trend estimates than shorter datasets previously used.

3. Recent heavy rain events in the past 10 years have contributed to spatial variability in trends in the nonstationary return value precipitation estimates across the Gulf and Southeast Coasts of the US.

To work toward addressing the hypotheses, the remainder of this thesis is organized as follows: Section 2 discusses the data and methods used for the analyses. The results are presented in Section 3. Final conclusions and a brief discussion of future work are given in Section 4.

2. DATA AND METHODS

2.1. Composite Station Construction

Daily precipitation data from the period 1890-2019 were acquired from stations located in a geographical area encompassing the Gulf and Southeastern Coasts of the US, ~26 °S, 35 °N, -100 °W, and -75 °E, that are included in the Applied Climate Information System database, which is maintained by NOAA's Regional Climate Centers. Most, but not all, of this data has undergone quality control as a part of the Global Historical Climate Network-Daily (GHCN-Daily) database (Menne et al. 2012). The quality control process is fully automated and performs well. Only 1%-2% of values flagged within GHCN-Daily are valid observations that have been flagged erroneously (Menne et al. 2012).

To assess the influence of recent storms on stationary return value estimates and nonstationary trend estimates, three separate datasets are considered. The first dataset includes all of the years between 1890-2019, while the remaining two data subsets are truncated at 2011 and 2000. These years were chosen as cutoff points because they align with the ending years of data used in NOAA Atlas 14 Volumes 9 and 2 respectively. This allows for a comparison between stationary estimates computed in this study and previously accepted stationary estimates from NOAA Atlas 14. Comparing trend estimates between datasets can also provide information about whether the increasing trend in extreme precipitation was enhanced in recent years as a result of heavier rain events such as several hurricanes and inland flooding events.

Before further assessing the quality of the station data, composite county stations were created. Compositing was done with the intention of obtaining both long record lengths and comprehensive spatial data coverage with the assumption that stations were within a similar meteorological setting to sample similar statistical precipitation distributions. This assumption should not introduce an overall bias because mountainous areas are avoided, and counties have an average size of 1,860 square kilometers, which is a small enough area to prevent any large climatological variations in precipitation distributions between stations. To create the county composites, stations within a county with no more than 31 missing days for a given year were identified. If only one station met that criterion, then that station's data were utilized for that year's block maximum. If more than one station met that criterion, then the station with the longest period of record was used. In cases where no stations met the missing day threshold, that year's block maximum for the county would be set to missing. County composites were discarded if they had fewer than 30 years of block maxima.

An additional three-part screening process was implemented here to eliminate any flawed extreme precipitation values that were not caught in the original GHCN-Daily quality inspections. The screening process focused on flagging spatial outliers for further investigation. A one-year block maximum of three-day precipitation was flagged if it exceeded the values reported at any neighboring stations for coincident periods by a factor of two or more or if the block maximum values were low outliers compared to surrounding stations. Next, the flagged block maxima were inspected manually to check for accuracy by looking at original observer forms, radar observations, neighboring

stations' reports, and other weather data. The data were assigned a quality control flag of "bad" if there was clear evidence of an error, "suspicious" if the value(s) were not blatantly wrong but had other evidence suggesting they were incorrect, such as an error in the observer form, "probably good" if there was no additionally sufficient evidence to remove the value, and "good" if the value was clearly represented in the original observer form and the report made meteorological sense. Any block maxima that were designated as "bad" or "suspicious" were removed from the data set prior to the analysis. Through this quality control process, 37 data points were removed out of a total of 60 flagged points and 66,113 block maxima points overall.

2.2. Analysis of Nonstationarity

The analysis of nonstationarity of the block maxima performed here follows similar procedures to the generalized extreme value (GEV) approaches as described in Martins and Stedinger 2000, El Adlouni et al. 2007, and Vu and Mishra 2019. A GEV distribution was fit to the block maxima while allowing only the location and scale parameters of the distribution to fluctuate with a covariate. The fit of the distribution was determined through the maximum likelihood estimation (MLE) method rather than L-moments due to its ability to evaluate nonstationary extreme value distributions (Martins and Stedinger 2000; El Adlouni et al. 2007). MLE has been shown to perform well with stationary and nonstationary analyses of extreme values (El Adlouni et al. 2007). The climextRemes package was used to perform the MLE (Paciorek et al. 2018). With the estimated return values from the GEV distribution, trends in the return values are

examined. Trends are quantified as the percent change in expected precipitation return values between 1960 and 2020. These return values are based on the entire quality-controlled dataset, with the assumption that the probability distribution is changing smoothly over time with changes to the covariate.

The change in water vapor holding capacity in the atmosphere, or the thermodynamic response, has been predicted to be the main driver of changes in extreme precipitation in the northern mid to high latitudes and is therefore the most relevant to this study (Pfahl et al. 2017). As such, global mean surface temperature is a valid and practical proxy option for a covariate (Sun et al. 2021). CMIP5 model mean global surface temperatures are chosen for this study as one covariate option, which Knutti and Sedlacek (2012) discussed as valid and consistent from earlier CMIP versions. CO_2 forcing can be used as another covariate (Risser and Wehner 2017). The natural log of atmospheric CO_2 concentrations provides an estimate for the forcing associated with CO_2 (Myrhe et al. 1998). By using the forcing of CO_2, volcanic eruptions are ignored, which can be beneficial since eruptions have a large effect interannually and will affect precipitation differently from greenhouse gases or even climate change (Mascioli et al. 2016). Therefore, we chose the log of atmospheric CO_2 as another covariate option for the purposes of this study. Figure 2-1 displays the time series of these nonstationary covariates. CMIP mid-year CO_2 historical concentrations (Meinshausen et al. 2011) through 2005 and the average annual Mauna Loa concentrations through present day are used. This data reports CO_2 concentrations with discrete steps between years, hence why the natural log of CO_2 concentrations in the time series reflects discrete steps.

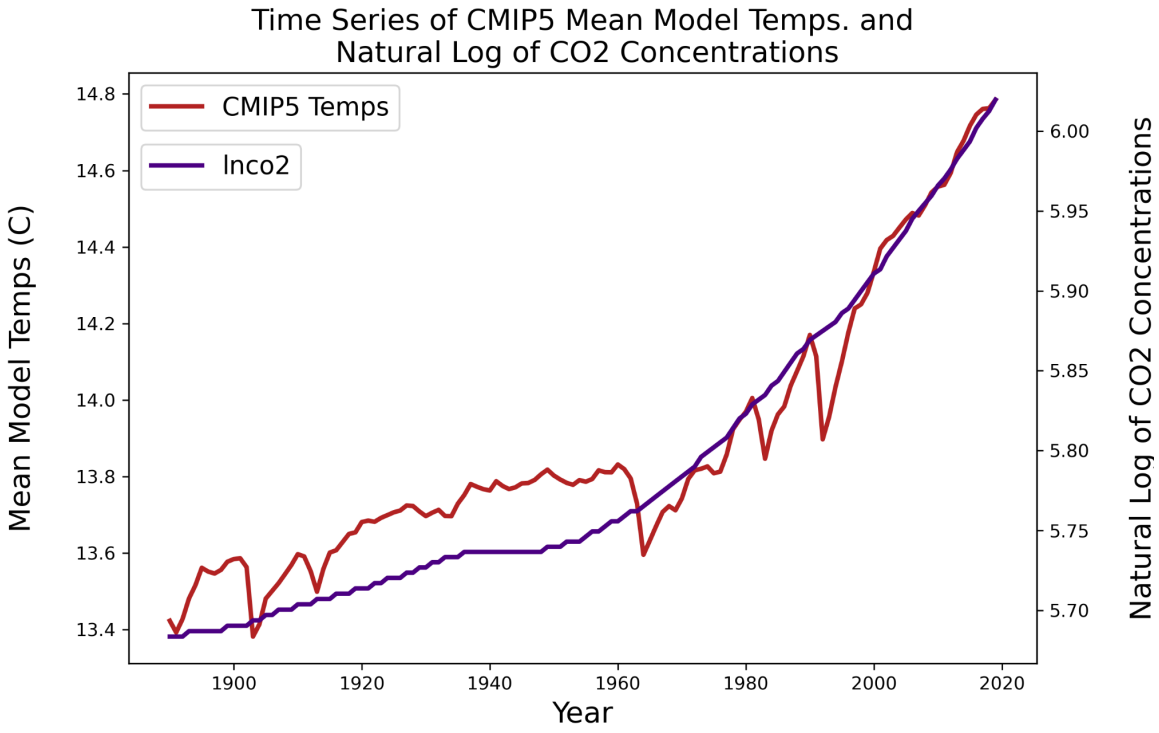

Figure 2-1: Time series of the nonstationary covariates chosen for this study. The dark red line shows the CMIP5 mean model temperature time series with associated y axis on the left side of the figure, and the dark purple line represents the natural log of CO2 concentration time series with associated y axis on the right side of the figure.

2.3. Substate Pooling

Previous studies have shown that aggregating precipitation station data yields more signal in trend estimates of extreme rainfall and a better estimate of the GEV shape parameter (Martins and Stedinger 2000; Fischer and Knutti 2016; Kunkel et al. 2020). Aggregation methods are employed for the purposes of this study as well. The county composite stations constructed for the block maxima rainfall were pooled together to create substate regions of approximately ten counties each and 20,000 square kilometers in area across the entire period of analysis prior to performing the GEV analysis. More

(fewer) counties are contained in a single region in states with smaller (larger) counties, such as Georgia (Texas). Pooled regions were designed to be compact and contain composite stations from a nearly uniform geographical setting for extreme rainfall, and a single GEV distribution was applied to each pooled region. Figure 2-2 depicts the pooled regions across the states used in this study, which are South & East Texas, Arkansas, Louisiana, Mississippi, Alabama, Georgia, Florida, South Carolina, and Central & East North Carolina.

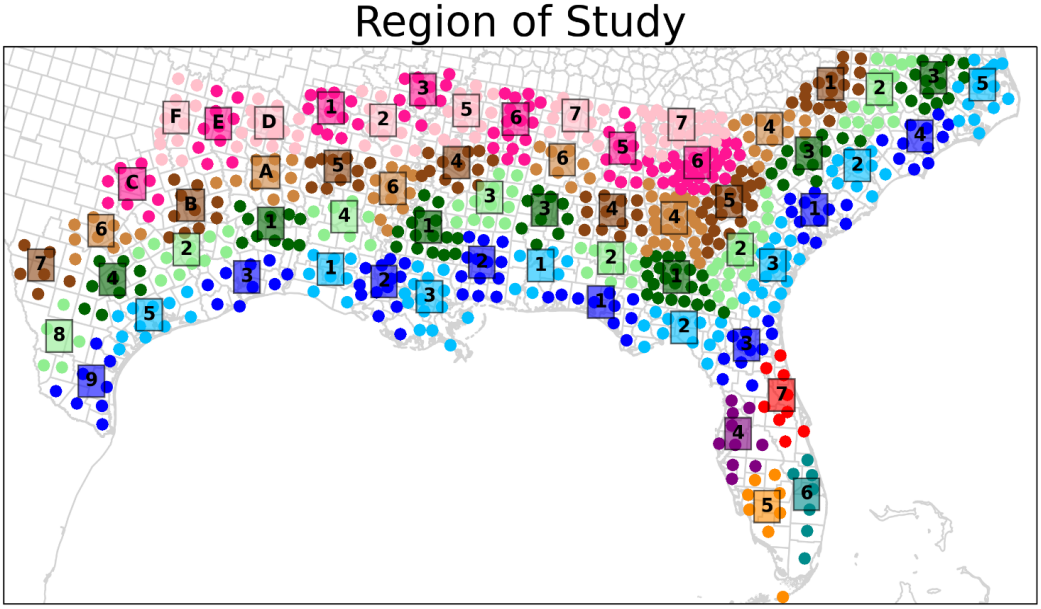

Figure 2-2: Boxes labeled with numbers and letters identify the pooled regions within a specific state. These labels do not connect across state boundaries. I.e., Region 1 in Texas does not relate to Region 1 in Louisiana. Individual dots within a specific region correspond to the county composites that make up that pooled area. Colors identify additional classifications of the pooled regions which are not considered in the present study.

2.4. Model Selection

In order to determine which of these statistical models (stationary or nonstationary) best fit extreme precipitation data, the Akaike Information Criterion (AIC) is often applied. The model with the lowest AIC value is considered to have the best fit (Vu and Mishra 2019). This method accounts for the number of terms estimated in the model as well as the likelihood function of the models, which can be calculated using the maximum likelihood estimation method (MLE), method of moments, or L-moments method. Prior studies have suggested that the MLE method using covariates in a generalized extreme value (GEV) model is a valid approach for acquiring the likelihood of models (El Adlouni et al. 2007; Martins and Stedinger 2000).

To avoid overfitting the data, the most parsimonious models must be chosen; fewer parameters that explain the behavior of the data are preferred in these models. The AIC was applied in this study to identify the models with the best parsimony. The natural log of atmospheric CO_2 held only marginally better AIC values as the covariate for the composite stations. CMIP5 mean model global surface temperature performed better for the pooled counties, according to the AIC statistics. The AIC results also helped identify which parameters should change with the covariate in the GEV model. For the composite stations, the mean AIC values and the spread of the AIC values were lower for the model where only the location parameter was varying. Contrastingly, for the pooled stations, the mean and spread of the AIC values were lower for the model where both the location and scale parameters were changing with the covariate. Based on these results, the models chosen for the nonstationary analysis were as follows:

1) A GEV fit to the logarithm of precipitation with the location parameter covarying with the CMIP5 mean model surface temperatures for composite stations
2) A GEV fit to the logarithm of precipitation with the location and scale parameters covarying with the CMIP5 mean model surface temperatures for pooled stations

The remainder of the analyses proceeds with the CMIP5 mean model surface temperature as the covariate.

2.5. Gaussian Process Model

To obtain information about the spatial patterns of the trends, and to compute confidence intervals of the mean trend, a Gaussian process model is applied. Gaussian processes are fields of variables that each have Gaussian probability density functions associated with them. The model accounts for the covariance between points, which provides the spatial element to the analysis. First, coordinates of the pooled trends were obtained from the latitude and longitude pairs for each of the regions in the area of study. From there, a Gaussian process model was fit to the pooled trends. The mathematical framework of the model can be seen in Equation 1:

$$Y(x) = \mu(x) + S(x) + e \qquad \text{Eq. (1)}$$

Y is the variable being observed, which corresponds to the pooled trends. The variable x defines the spatial location, latitude and longitude pairs, of the trends. The

term, $\mu(x)$, is equivalent to a covariate term multiplied by a beta estimate across the spatial domain. $S(x)$ is the stationary Gaussian process, and e is an error term. The key terms from the output for estimating the aggregate of the pooled trends are the beta term, which represents the mean trend, and the beta variance, i.e., the variance of the mean trend. Bounds of the confidence interval are calculated by taking the mean trend and adding or subtracting 1.96 multiplied by the square root of the mean trend variance. The value 1.96 is the z-value for the significance level of 0.05, which corresponds to a 95% confidence interval.

3. RESULTS

3.1. Stationary Analysis

To establish the validity of the methods described in Section 2, a stationary GEV analysis was performed with a similar approach to NOAA Atlas 14. The GEV parameters were acquired from the previously mentioned MLE, and no covariates were used since the analysis was stationary. Return values were first calculated from the block maxima in the county composite stations for 2-yr and 100-yr return periods.

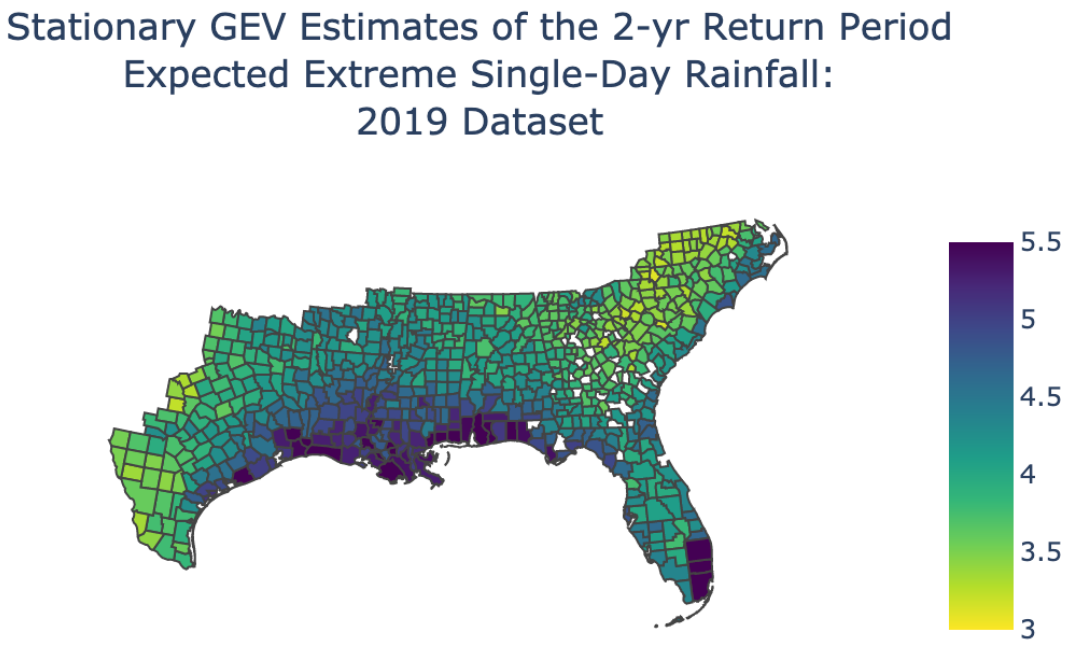

Figure 3-1: Composite station 1-day rainfall amounts (inches) from the quality controlled full dataset under a stationary model for the 2-yr return period

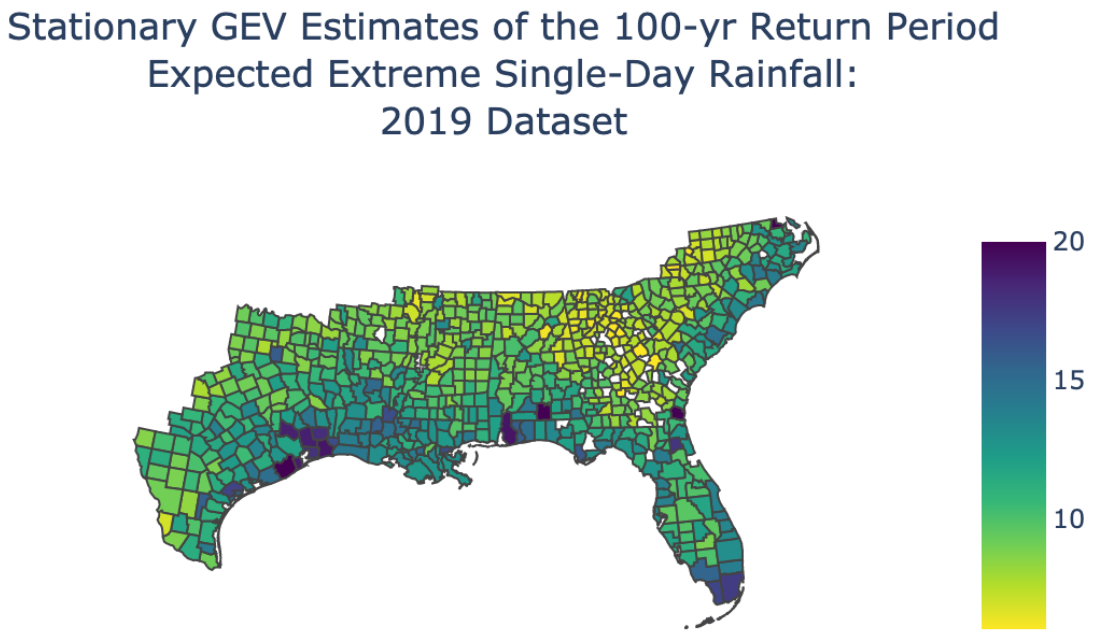

Figure 3-2: Same as Fig. 3-1, except this is for the 100-yr return period

The 2-yr composite stationary 1-day duration return values are plotted in Figure 3-1. Higher return values exist along the Gulf Coast. The 2-yr return values are spatially more coherent than the 100-yr composite 1-day values (Fig. 3-2). This reflects the idea that return values toward the middle of the cumulative GEV distribution have lower uncertainty than those at the tails. Pooling by region is sufficient to produce spatially coherent return value estimates even at the longer return periods using these methods, which is apparent in the systematic reduction in return values with distance inland (Fig. 3-3; Fig. 3-4). However, there are two exceptions to this reduction in return values,

which occur over northwestern South Carolina and the southern Edwards Plateau region in Texas. These exceptions could be a result of topographic effects in those areas.

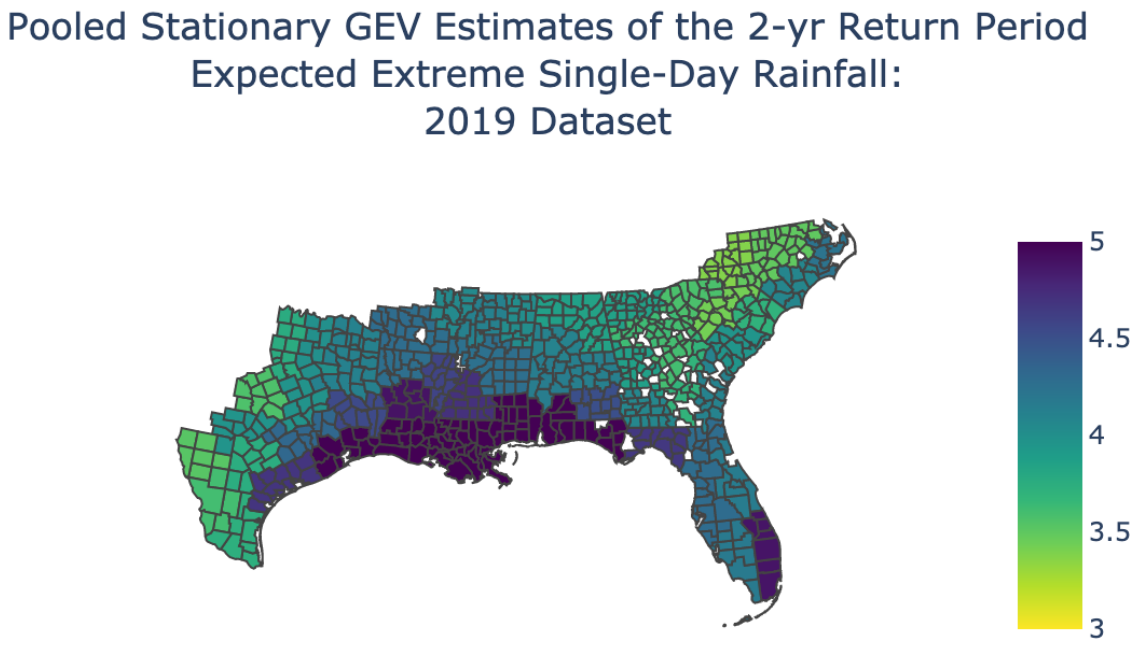

Figure 3-3: Pooled stations 1-day rainfall amounts (inches) from the quality controlled full dataset under a stationary model for the 2-yr return period

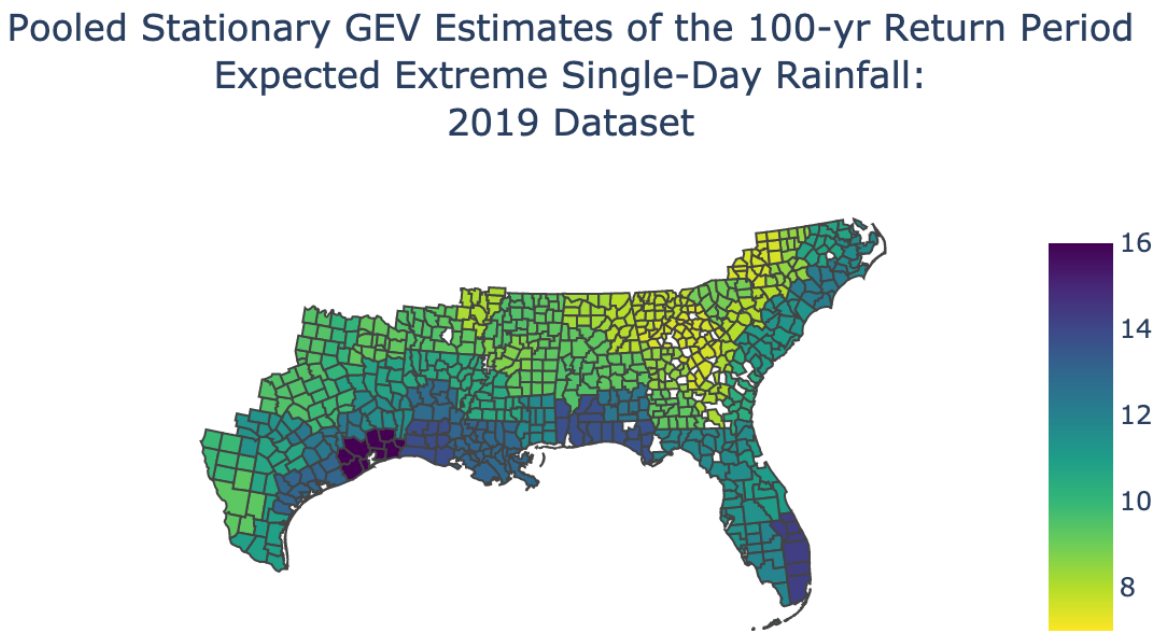

Figure 3-4: Same as Fig. 3-3, except this is for the 100-yr return period

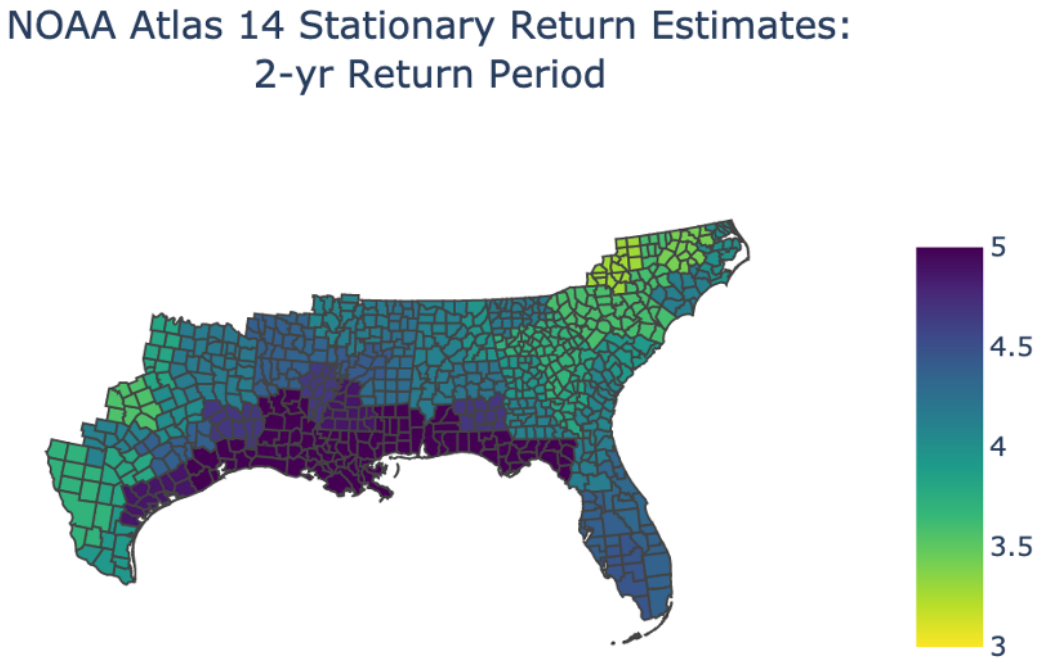

Figure 3-5: Pooled stations 1-day rainfall amounts (inches) from the NOAA Atlas 14 Volume 2 (North and South Carolina), Volume 9 (Alabama, Arkansas, Georgia, Louisiana, Florida, and Mississippi), and Volume 11 (Texas) datasets under a stationary model for the 2-yr return period. Data end years for each volume were 2000, 2011, and 2019, respectively

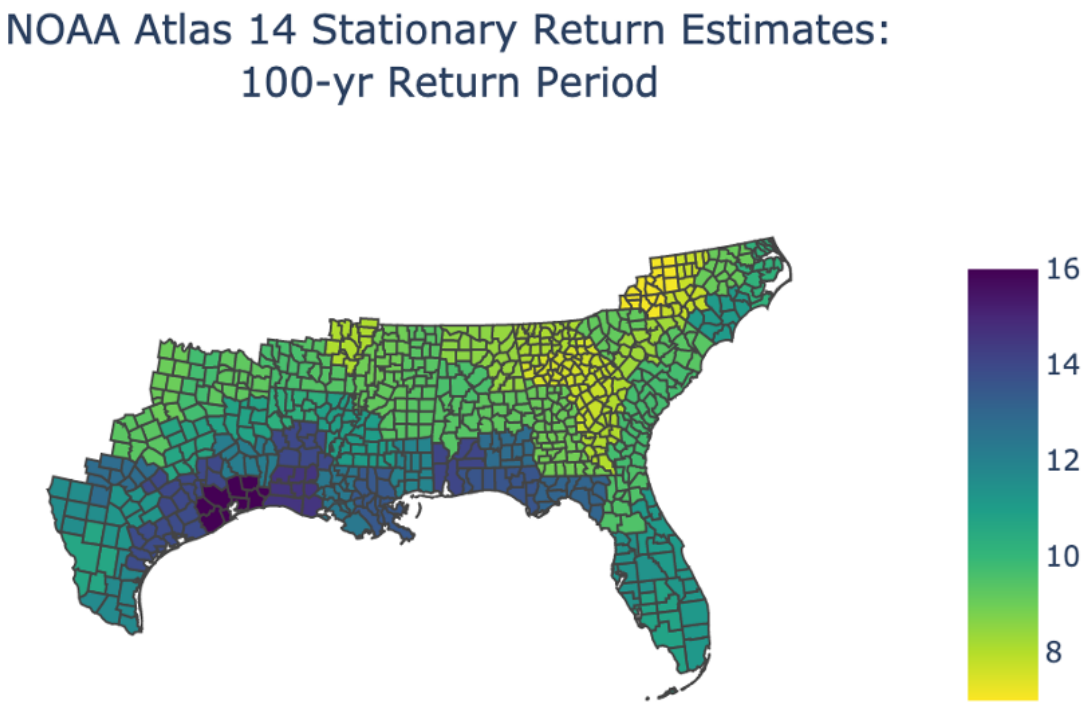

Figure 3-6: Same as Fig. 3-5, for the 100-yr return period

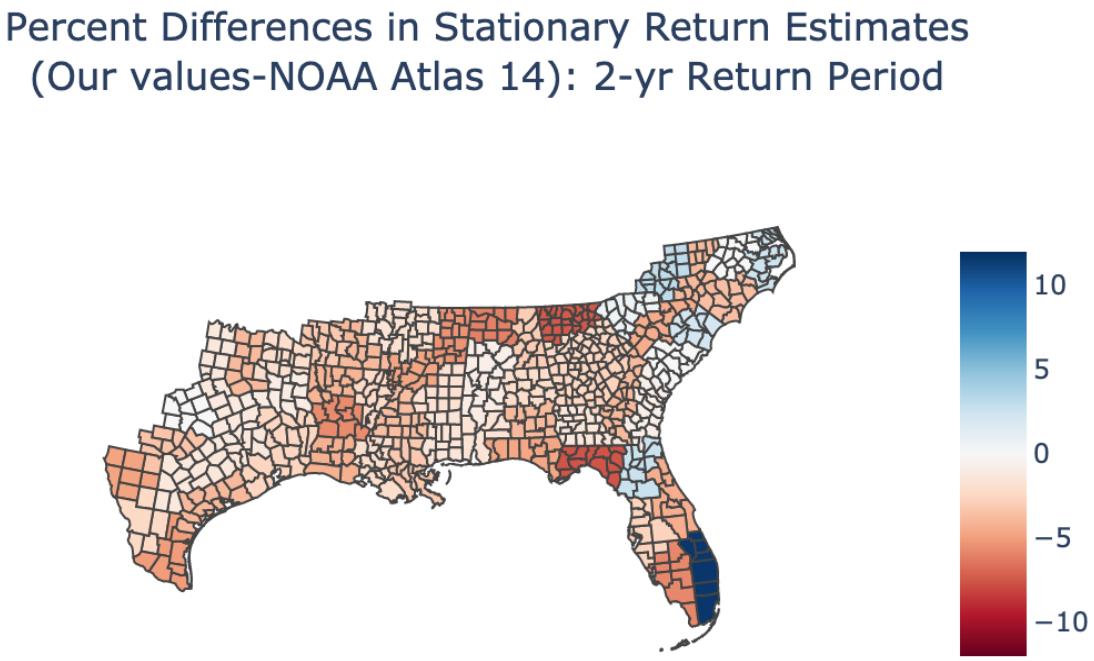

Figure 3-7: Percentage differences in pooled stations 1-day rainfall amounts between our calculated stationary return values and NOAA Atlas 14 values shown in Fig. 3-5 for the 2-yr return period. The comparison is made between analyses with the same data time cutoffs as mentioned in Fig. 3-5. E.g., the North Carolina & South Carolina differences reflect the differences between our calculated return values using the dataset cut off in 2000 and the NOAA Atlas 14 Volume 2 values which also used data through 2000.

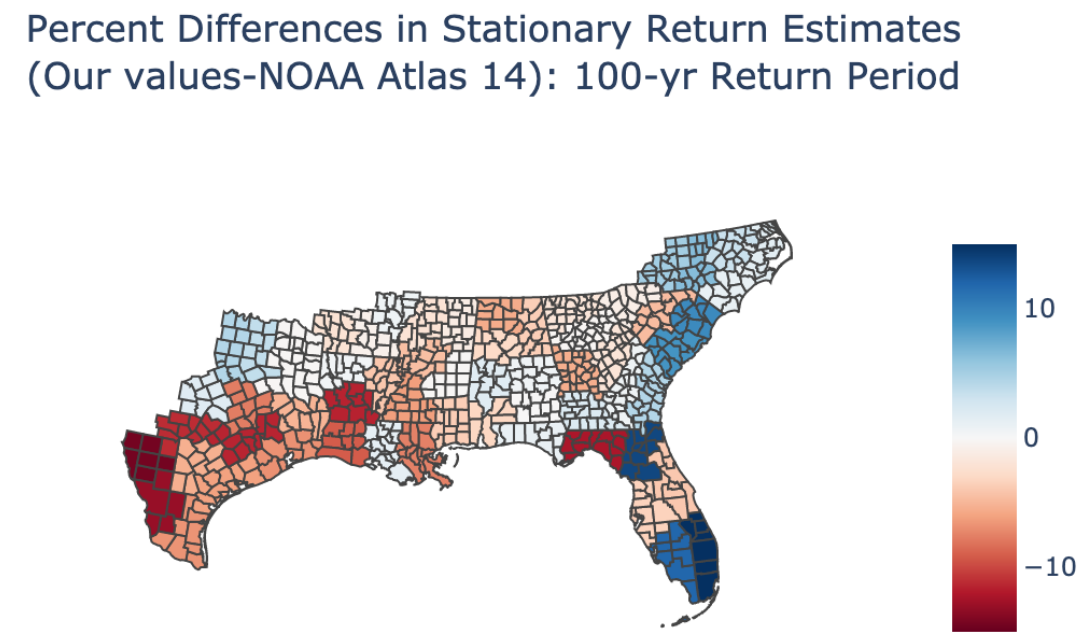

Figure 3-8: Same as Fig. 3-7, for the 100-yr return period

Overall, the stationary return value pattern calculated using the methods outlined here appears to be consistent with prior stationary estimates. A direct comparison to NOAA Atlas 14 stationary estimates demonstrates that the methods performed in this study are generally valid. The return values from Volume 2 (Fig. 3-5; Fig. 3-6) are similar to the return values calculated for this study. The data were truncated at the year 2000 because NOAA Atlas 14 Volume 2 was produced using data through that year. For example, North Carolina Region 3, which can be identified from Figure 2 in section 2, has a pooled 2-yr return period value of 3.42" (Fig. 3-5) and a 100-yr return period value of 9.38" (Fig. 3-6). NOAA Atlas 14 estimated the average return value for a 2- and 100-yr return period for that region as 3.42" and 9.08", respectively, which led to no

difference between the values calculated in this study compared to those Atlas 14 estimates at the 2-yr return period (Fig. 3-7) and a 3% difference at the 100-yr return period (Fig. 3-8). Similarly, the estimates for South Carolina Region 4 for this study's calculations were 3.61" and 9.1". Those same return values from NOAA 14 were 3.59" and 9.19", resulting in a 1% difference and a -1% difference at the 2- and 100-yr return periods. Note that positive differences indicate that the present values are larger than Atlas 14 while negative differences indicate that Atlas 14 estimates are larger.

Return value estimates were also fairly comparable for states in Volume 9, which had a data cutoff year in 2011. Louisiana Region 3, located on the coast, has regional values of 5.16" for the 2-yr return period (Fig. 3-3) and 12.48" for the 100-yr return period (Fig. 3-4). From NOAA Atlas 14, these values were roughly 5.33" and 13.50" (Fig. 3-5; Fig. 3-6) Furthermore, Arkansas Region 2 had average pooled values from NOAA Atlas 14 as 4.36" and 9.43" while the values computed in this study are 4.19" and 9.36" respectively. The associated percent differences for Louisiana Region 3 at the 2- and 100-yr return periods were -3% and -8%, while Arkansas Region 2 had differences of -4% and -1% (Fig. 3-7; Fig. 3-8). The largest differences between the stationary estimates occur in Florida Region 6 where the differences at the 2-yr return period are 12% and 26% at the 100-yr return period.

Similar return value estimates between this work and NOAA Atlas 14 are found for the more recent Volume 11 as well. For example, Texas Region A, located in eastern Texas, has a 1-day duration pooled stationary return value for the 2-yr return period of 4.12" (Fig. 3-3) and for the 100-yr return period of 10.78" (Fig. 3-4). NOAA Atlas 14

reports return values of approximately 4.16” for the 1-day duration 2-yr return period (Fig. 3-5) and 10.80” for the 100-yr return period (Fig. 3-6) in Region A. This resulted in a percent difference of -1% and ~0% for the associated return periods (Fig. 3-7; Fig. 3-8). From these comparisons between prior well-established work and the current study, it can be seen that the estimates presented here tend to be only slightly different than the NOAA Atlas 14 estimates, with the vast majority of regional estimates having negative differences. Overall, the percentage change between current values and those in NOAA Atlas 14 vary from -8% to 12% for the 2-yr return period and -15% to 26% for the 100-yr return period. Interestingly, the largest positive differences occur along the Atlantic Coast. Differences exist between these estimates and NOAA Atlas 14 likely due to a few reasons. First, Atlas 14 does not use composite stations in the statistical analysis. Time series from individual stations were used, and the GEV model was fit to each time series separately. Furthermore, when the GEV estimates from each time series were aggregated together in Atlas 14, it was done through the examination of the proximity of stations to each other, elevation, and other factors. Here, the regions are defined geographically by hand prior to fitting the GEV distribution to the data. A third reason differences exist between these estimates and Atlas 14 is due to the difference in GEV parameter calculation methods. Atlas 14 used L-moments, while this study uses the MLE method. Despite this, the differences between return values are not sufficient to suggest that our methods of calculating them are poor.

3.2. Nonstationary Analysis

The nonstationary analysis of block maxima rainfall, as described in section 2, allowed for an examination of the trends in extreme rainfall across the area of study. Figure 3-9 depicts the 100-yr composite station trend patterns for 1-day precipitation durations. Only the 100-yr return period composite trends are shown here because only the location parameter is changing in the GEV distribution for the composite stations. This means that the return values must change by similar proportions for each return period since the distribution is only shifting along the x-axis when the location parameter changes, while the width of the distribution is constant. It is important to note that this is true only if the GEV is fit to the logarithm of precipitation, which is what is done in this study. Therefore, there is a negligible difference between the 2-year return period and the 100-year return period at the composite station level. The trends vary from ~ -30% to ~ +60% across the area of study. Larger positive trends are found across Louisiana, Mississippi, East Texas, and coastal North Carolina. However, there are also numerous composite stations that highlight strong negative trends throughout this area. Georgia, for example, reflects this juxtaposition well with several negative trends interspersed among positive trends; record lengths can be much shorter in Georgia though, which can leave more noise in the trend estimates. The composite trend patterns demonstrate the magnitude of the natural variability present within the block maxima precipitation through the spatial variability in the trends, which can be interpreted here as natural variability since the trends at this small scale do not account for the broader physical changes that occur as the global temperature increases.

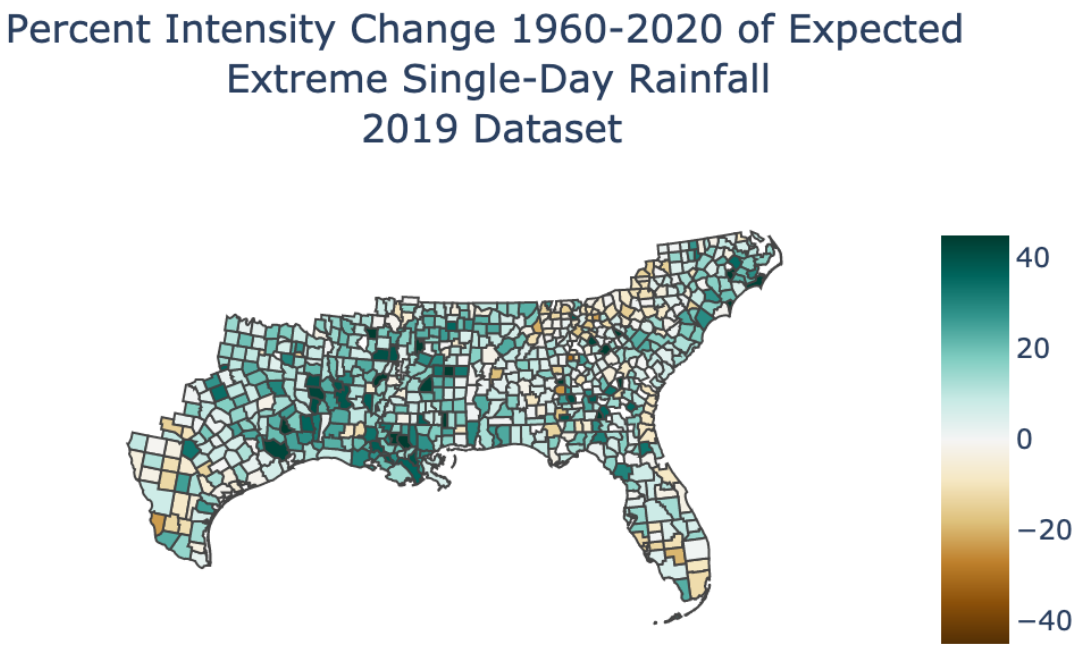

Figure 3-9: Percentage changes in nonstationary composite station estimates of expected 1-day return values between 1960 and 2020 for the 100-yr return period

Patterns within 1-day duration trends across the area of study become more apparent in the pooled regions. Pooled trends for the 2- and 100-yr 1-day duration precipitation return values are shown in Figures 3-10 and 3-11 respectively. The trends for the 2-yr return period show less spatial variability than the 100-yr return period trends because they are less affected by event outliers. A discussion on the impact of recent storms on the trend estimates will be discussed later in this section.

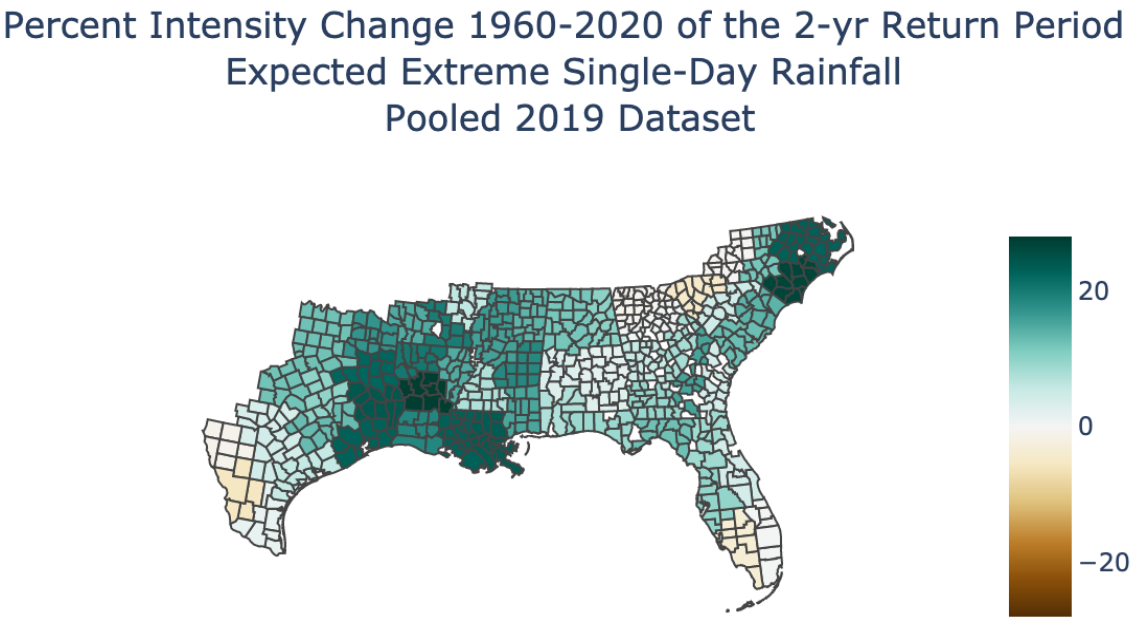

Figure 3-10: Percentage changes in nonstationary pooled station estimates of expected 1-day return values between 1960 and 2020 for the 2-yr return period

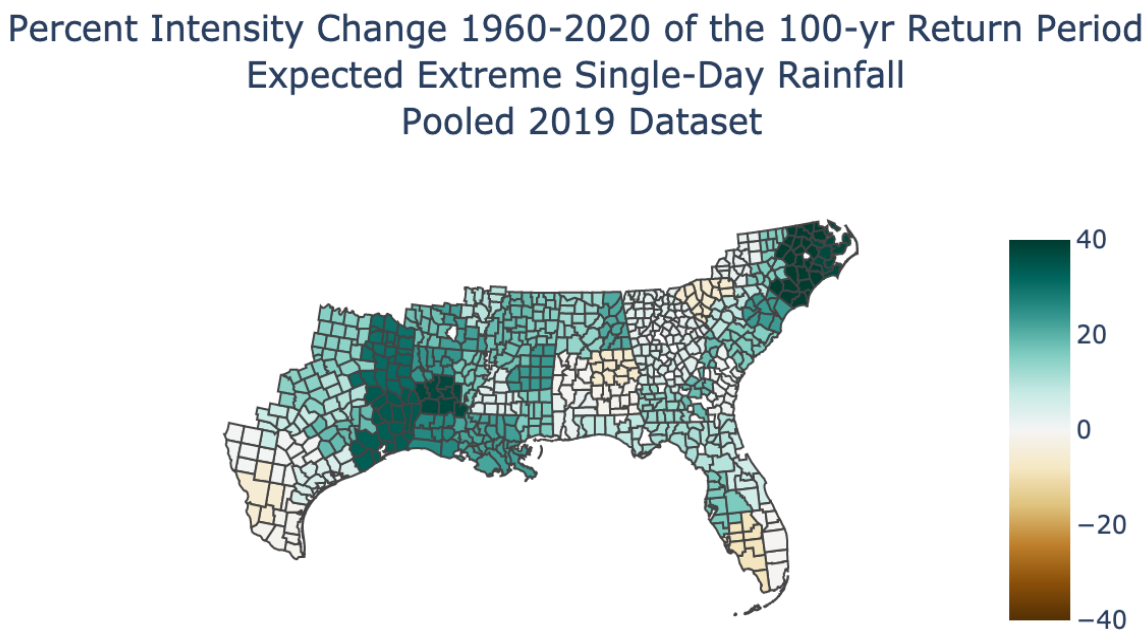

Figure 3-11: Same as Fig. 3-10, for the 100-yr return period

Using the natural log of CO_2 concentrations as the covariate yields similar trend results. The broad patterns of the trends are generally the same both with the composite station trends and the pooled regions (not pictured). The trends from the two covariates are mainly within 10% of each other. Agreement between trends from both the mean model temperatures and natural log of CO_2 covariates indicates that the choice of covariate did not greatly affect the extreme rainfall return value estimates for this nonstationary analysis.

3.3. Impact of Recent Storms

To assess the extent to which recent weather events have impacted the stationary and trend estimates of extreme precipitation since NOAA Atlas 14, the truncated datasets are used. The same analyses are performed on the shortened datasets, and the

results are then compared to those using the full dataset. For the purpose of this discussion, only the 100-yr return period results will be highlighted to focus on the tail of the probability distribution. Differences between the stationary return value estimates from the data through 2011 and 2019 for 1-day duration precipitation are shown in Figure 3-12 and Figure 3-13. Notably, in the pooled estimates there are several regions with positive differences (2019 values are higher when there is a positive difference) (Fig. 3-12). These positive differences are approximately 1, corresponding to 1 inch of precipitation, at the highest locations. The differences are understandably more spatially varying in the composite stations (Fig. 3-13). Locations in southeastern Texas and the

As the data record is shortened further, the differences between the stationary estimates are magnified. This is clearly evident in Figure 3-14 and Figure 3-15, which display the differences in stationary estimates between data years ending in 2000 and 2019. More negative differences (2019 values are lower) are apparent in the pooled map (Fig. 3-14) than there are in the 2019-2011 map. The largest negative difference is roughly 2 inches, and the largest positive difference is roughly 1 inch. Amplified differences even in the stationary return values emphasize the importance of updating extreme precipitation estimates for planners.

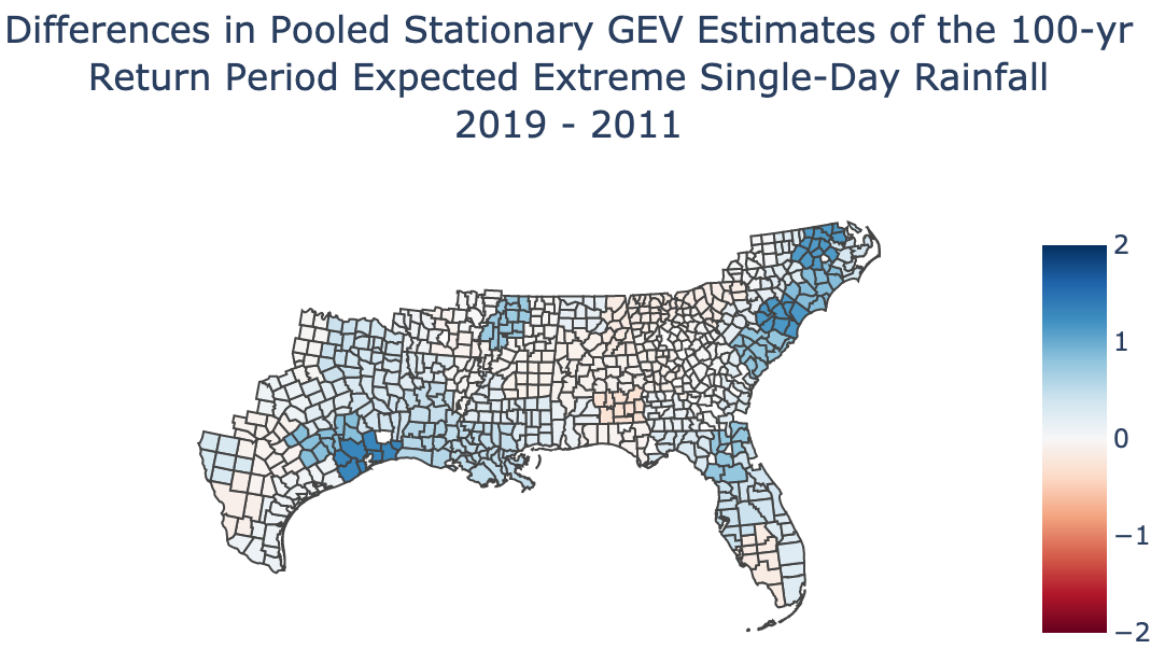

Figure 3-12: Differences in stationary estimates of 1-day 100-yr return values (inches) between the 2011 and 2019 datasets for the pooled stations

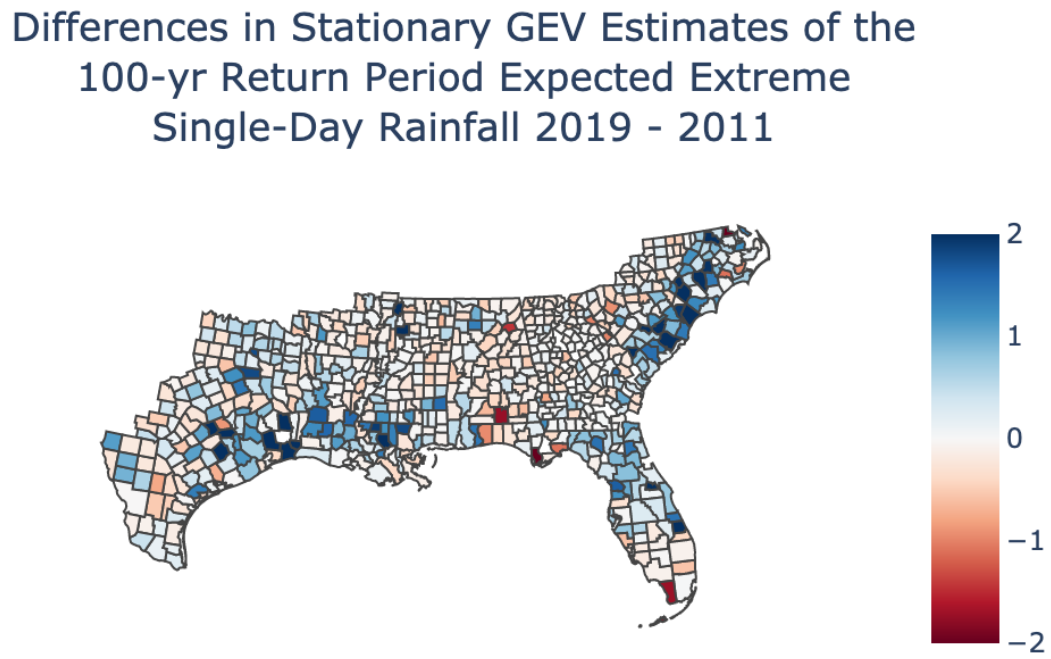

Figure 3-13: Same as Fig. 3-12, for the composite stations

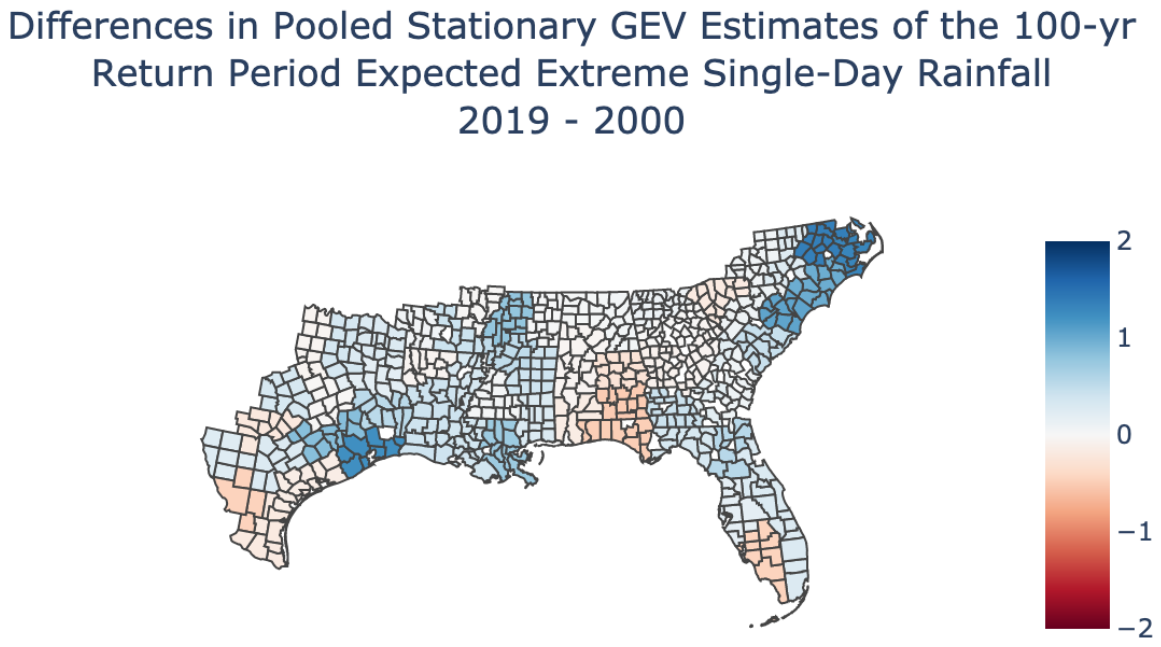

Figure 3-14: Same as Fig. 3-12, except this is showing the differences between the 2000 and 2019 datasets

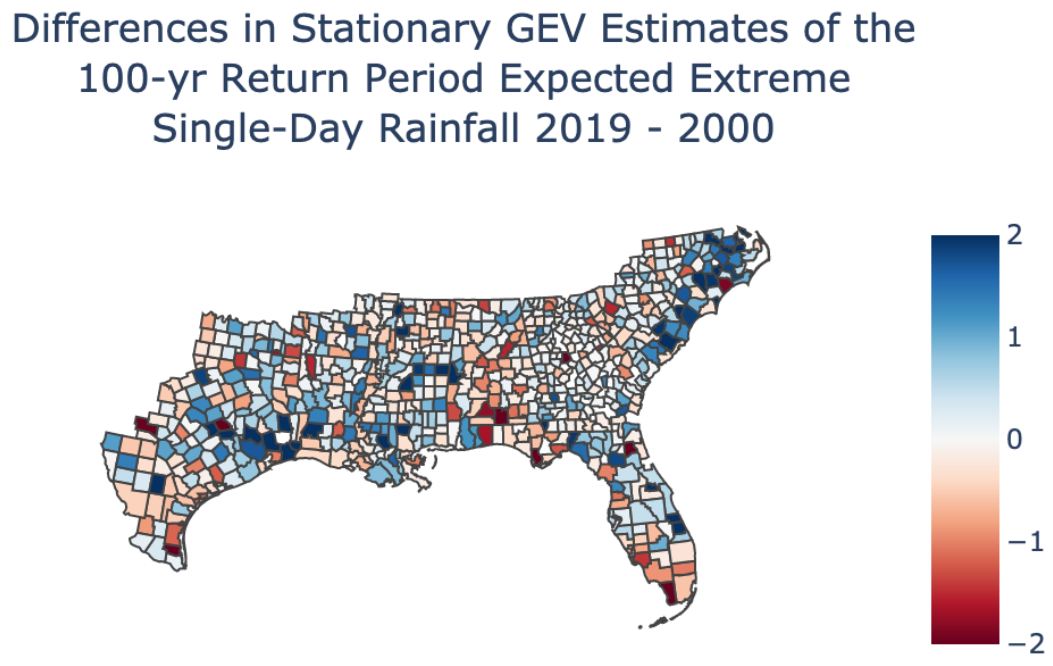

Figure 3-15: Same as Fig. 3-14, for the composite stations

Recent storms influence the trends in the nonstationary extreme precipitation as well. Figures 3-16 and 3-17 display the percentage changes between the trend estimates from the 2011 and 2019 data for 1-day duration precipitation. It is relevant to note that while there are negative values on these difference plots, that does not imply that the trends in 2011 or 2000 were decreasing. The differences note the changes in trend magnitude between the datasets, which means that while both 2011 and 2019 may show an increasing trend in the data, if the trend was larger in magnitude in 2011 than in 2019, then that difference value would be negative. The effect on the difference in return values between 1960 and 2020 is larger than the effect on the stationary values themselves. Impacts from the recent events have similar signs between the trends and stationary estimates, as expected. 100-yr return period or smaller spatial scale precipitation estimates specifically are much more influenced by event outliers as they affect the tails of the probability distribution more than the center of the distribution. The differences in these trends vary from -34% to +42% for the composite stations (Fig. 3-17). The differences in pooled trends ranges from -23% to +22% (Fig. 3-16).

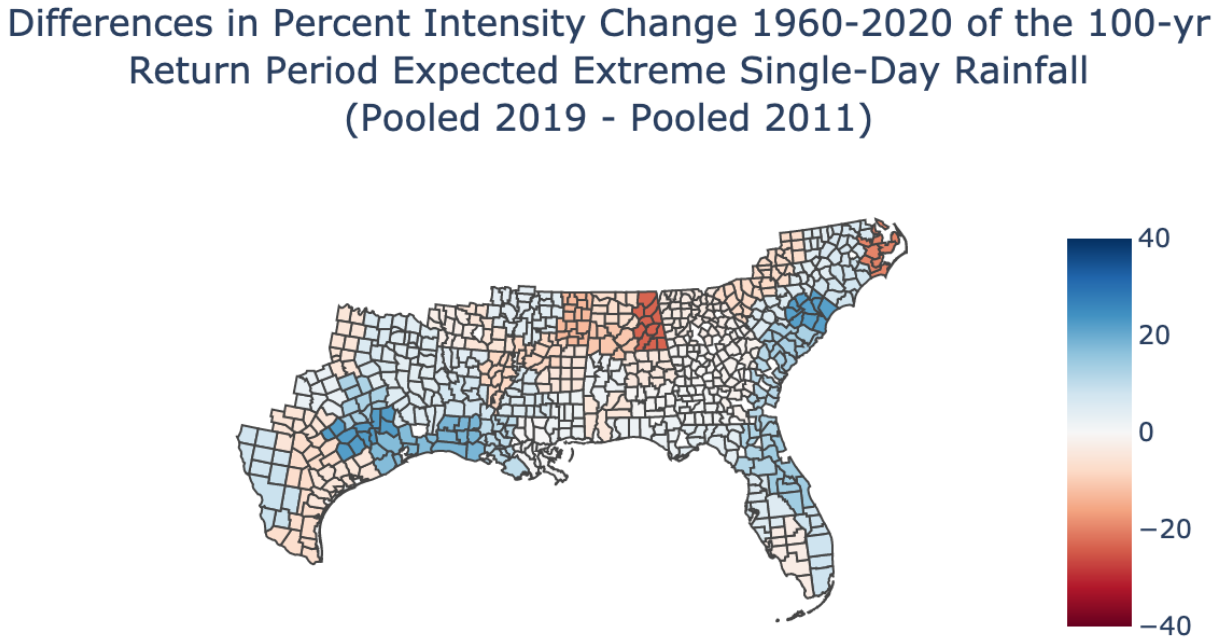

Figure 3-16: Percentage differences in nonstationary trend estimates of 1-day 100-yr return values between 2011 and 2019 datasets for the pooled stations

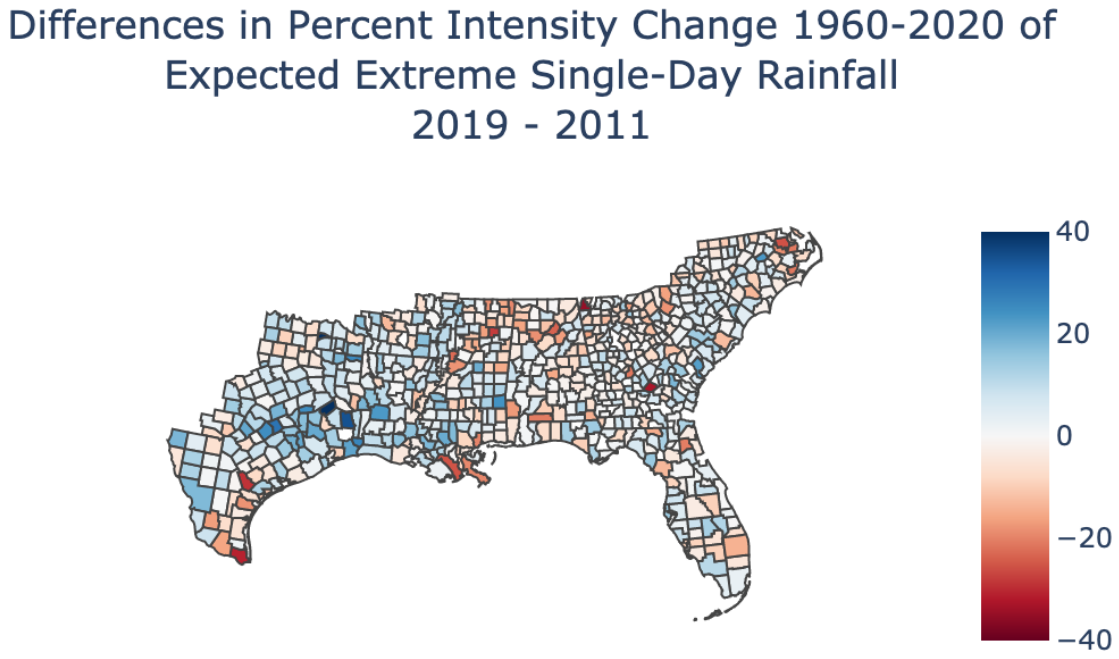

Figure 3-17: Same as Fig. 3-16, for the composite stations

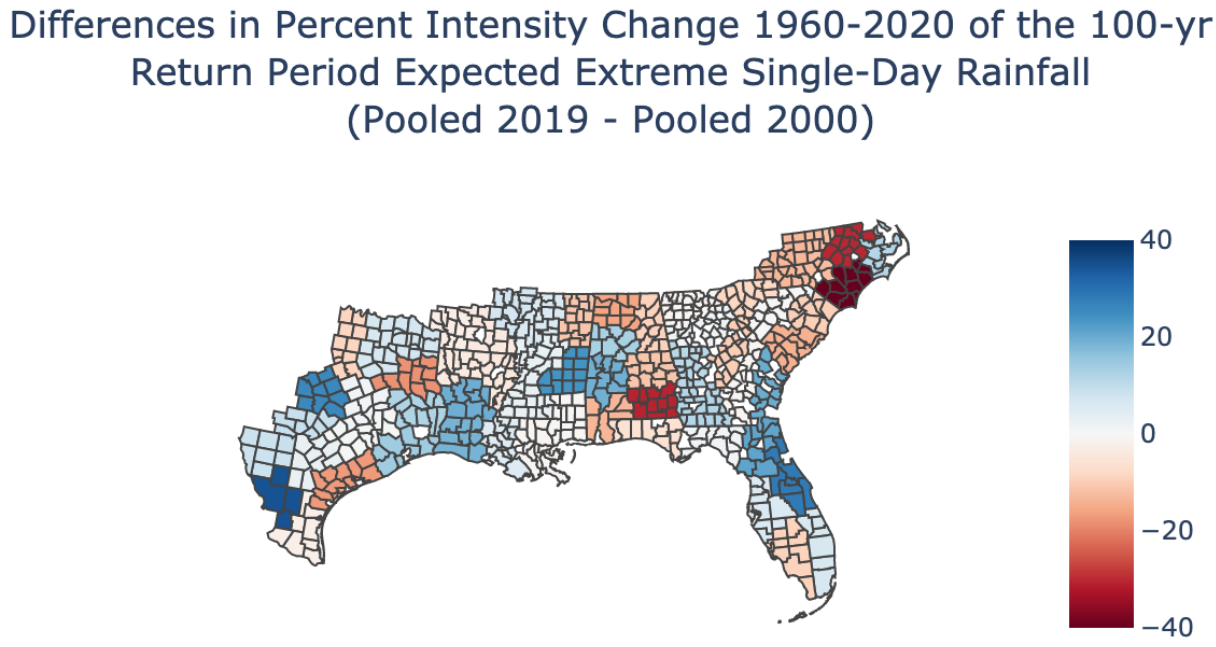

Figure 3-18: Same as Fig. 3-16, except these are the differences between the 2000 and 2019 datasets for the pooled stations

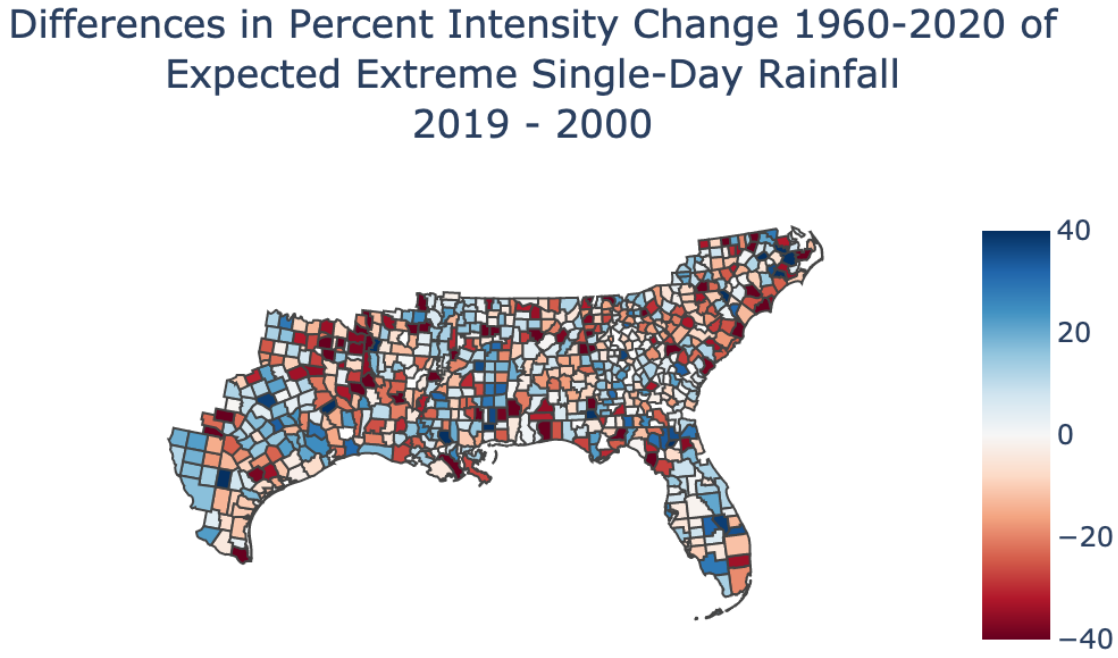

Figure 3-19: Same as Fig. 3-18, for the composite stations

Larger differences in the trends exist between the full dataset and the dataset that ends in 2000. The pooled trend differences vary from -42% to +34% (Fig. 3-18) while the composite station trend differences vary from approximately -60% to +50% (Fig. 3-19). These trend differences, both for the dataset that ends in 2000 and 2011, further highlight the need for Atlas 14 updates in states presented here, especially North and South Carolina whose Atlas 14 volume used data through 2000. Nonstationary trend estimates, as well as the stationary estimates discussed earlier in this section, can be vastly different when using shorter periods of record.

3.4. Aggregated Trends

From the pooled trend estimates for extreme precipitation, the next step involves examining the aggregate of these trend estimates using spatial statistics. The goal is to acquire the estimated mean trend across the entire spatial domain and confidence intervals of the mean trend for the 2- and 100-yr return periods using all three datasets separately. Estimates of the beta term, beta variance, and bounds of the confidence intervals for the 2- and 100-yr return periods are summarized in Table 3.4.1. Using the full dataset, it can be seen that the estimated mean trend is ~9% for the 2-yr period and ~13% for the 100-yr return period. The confidence intervals are wider for the dataset ending in 2000 at both return periods than the 2011 and 2019 datasets. Similarly, the beta estimate for the 2-yr return period from the 2000 dataset is larger than the estimate for 2011 and 2019. However, at the 100-yr return period, the mean trend estimate for the full dataset, ~13%, is larger compared to the other datasets which are ~12%. The

confidence intervals at the 100-yr return period are wider for the full dataset than the 2011 dataset, but narrower than the 2000 dataset. Statistically, the confidence intervals for the differences between the 2- and 100-yr return period trends are more robust than the intervals of the raw trends themselves (not shown). The intervals for the three datasets, 2019, 2011, and 2000, are approximately (-0.13, 6.7), (-3.4, 10.9), and (-4.1, 9.3). Negative differences highlight when the 2-yr return period trend was larger than the 100-yr return period trend, while positive differences reflect the opposite.

End year of dataset	Return Period	Beta estimate	95% CI lower bound	95% CI upper bound	Beta variance
2019	2-yr	8.89	0.853	16.918	16.796
2019	100-yr	12.89	3.174	22.606	24.573
2011	2-yr	8.80	2.989	14.602	8.776
2011	100-yr	11.85	3.218	20.491	19.416
2000	2-yr	9.43	2.096	16.766	14.005
2000	100-yr	12.29	0.0922	24.478	38.700

Table 3.4.1: Each ending year of the three datasets are displayed with their corresponding return periods, beta estimates of the average trend over the entire study area from the Gaussian process model, and confidence intervals computed from the output of the Gaussian process model. Trends are expressed as percentages.

In addition to the confidence intervals computed for the aggregate of the pooled trends, it is important to consider how the trend estimates and the associated confidence intervals compare at an intermediate aggregation level to those found across the entire domain of pooled stations. The confidence intervals calculated for the intermediate aggregation trend estimates not only describe the uncertainty associated with the trends

at that level of aggregation, but they also help inform how robust the climate-driven trend is at a smaller aggregation. To do this, the pooled regions were divided into the Gulf Coast only and the Southeast Coast only. The Gulf Coast was defined as all Alabama regions, all Arkansas regions, Florida regions 1, 2, and 3, all Louisiana regions, all Mississippi regions, and all Texas regions. The Southeast Coast was defined as all Georgia regions, all South Carolina regions, and all North Carolina regions. Averages of the pooled trends across each of these aggregated subdivisions were computed for the 2-yr and 100-yr return periods. This was done separately for each dataset ending year. Table 3.4.2 shows the average trends for each aggregated region and the 95% confidence intervals computed from the Gaussian process model output in each dataset. The confidence intervals of the 2-yr return period trends for the 2019, 2011, and 2000 datasets are approximately (9.6, 12.7), (8.2, 10.8), and (12.3, 13.1) respectively. Comparatively, the confidence intervals of the 100-yr return period are (14.3, 14.9), (13.1, 13.2), and (10.1, 21.7). The average trends for these aggregated regions are larger than those found for the aggregates of the pooled trends. Furthermore, the confidence intervals of these additional aggregates are narrower than the intervals produced from the pooled trends (Table 3.4.2). However, these intervals are so narrow because there are only two data points being used in the spatial model, and less data will shrink confidence intervals. Aggregated regions at this scale are therefore not beneficial for ascertaining the climate-driven trend from noise.

End year of dataset	Aggregated region	2-yr RP Trends	100-yr RP Trends	2-yr RP 95% CI	100-yr RP 95% CI
2019	SE Coast	9.565	14.785	(9.047, 12.765)	(14.291, 14.864)
2019	Gulf Coast	12.248	14.371		
2011	SE Coast	8.562	13.164	(8.203, 10.782)	(13.154, 13.223)
2011	Gulf Coast	10.423	13.213		
2000	SE Coast	12.982	20.149	(12.293, 13.094)	(10.078, 21.778)
2000	Gulf Coast	12.405	11.707		

Table 3.4.2: Each ending year of the three datasets are displayed with their corresponding aggregated regions and trends at the 2- and 100-yr return period. 95% confidence intervals, which were calculated using the output from the Gaussian process model, for each year and return period are presented as well. Trends are expressed as percentages.

4. CONCLUSIONS

Extreme rainfall has been a topic of societal importance in the United States, particularly in response to events such as Hurricane Harvey, but changes in extreme rainfall are of emerging concern. Robust and scientifically sound trend estimates of extreme precipitation are crucial for emergency managers, city planners, engineers, and policy makers as global temperatures continue to rise. While past and current studies do address trends in extreme rainfall from observational datasets, this study aims to focus on such trends across the Gulf and Southeastern Coasts of the US, specifically working toward improving upon existing analytical methods of evaluating the climate-driven trends in extreme precipitation. To do this, precipitation station data are acquired from 1890-2019 using the Applied Climate Information System from NCEI. Stations are first composited in each county, and then multiple composite stations are treated as a single set of observations to create pooled regions in each state. GEV models are fit to the logarithm of precipitation for both the composite stations and the pooled regions using CMIP5 global mean surface temperatures as the covariate for the nonstationary analysis. Through the analysis, stationary extreme rainfall return values are compared to the NOAA Atlas 14 stationary estimates. Trends in the nonstationary return values are calculated and compared across datasets of different time cut-offs and are further inspected using spatial statistics.

The results presented in this thesis are comparable to NOAA Atlas 14 stationary return value estimates. Daily pooled stationary return values calculated in these analyses

appear to be generally smaller than the pooled stationary values from NOAA Atlas 14 Volumes 2, 9, and 11 for both the 2- and 100-yr return periods. These differences in the exact values do not appear to be problematic, especially considering the overall patterns of the stationary values across the Gulf and Southeast are consistent between the NOAA Atlas 14 volumes and the current study. Disparities are apparent due to differences in the regionalization of the data, GEV parameter estimation methods, and treatment of the data prior to fitting the GEV distribution to it.

Directly comparing trend estimates between this work and previous literature is not entirely beneficial since different methods for calculating trends and definitions of trends can lead to widely varying results. However, one can consider how the magnitudes of the trends, the methods used to compute the trends, and the information gathered from the trends compare between this thesis and preceding studies. Previous observational studies have shown that the Southeastern US has experienced increases in the frequency and intensity of extreme precipitation. Increasing intensity is reflected in the trends of extreme precipitation return values. The trends computed here for the full precipitation dataset (data through 2019) predominantly support those patterns, especially in the pooled regions. Pooled trend values vary from -5% to 27% for the 2-yr return period and from -8% to 49% for the 100-yr return period. Of the 60 pooled regions, four exhibit negative trends at the 2-yr return period while six exhibit negative trends at the 100-yr return period. The largest positive trends are found across eastern Texas, Louisiana, and the coast of North Carolina.

This pattern of positive trends across the Gulf and Southeastern Coasts of the US does broadly align with prior studies, even studies that aggregated stations to a larger level. However, there are key differences between this thesis and previous studies. For example, Kunkel et al. (2020) examined annual trends in the 1-day return values that exceeded a certain value at a given return period. The highest return period considered was 20 years, so the 20-yr return value was computed. Trends were then calculated for the values that exceed that 20-yr return value and for the other return periods considered. The annual trend (% per decade) from 1949-2016 for the 1-day return values that exceeded the 2-yr return period value was 4% in Kunkel et al. (2020), while this study's aggregated actual 1-day 2-yr return period trend from 1890-2019 for the Southeast Coast was ~10%. It is also important to note that Kunkel et al. (2020) used region definitions that are different from the ones presented here. Furthermore, Kunkel et al. (2020) did not quantify the confidence intervals of their trends, while this study did.

Wu (2015) also computed trends in daily extreme precipitation in the Southeast US while using nearly identical climate divisions as Kunkel et al. (2020). Before pooling the data into the climate regions, the annual maximum precipitation at each station was normalized by the annual maximum precipitation mean, which is one difference between that study and the current work. Percent changes in daily precipitation return values between the 1951-1980 period and the 1981-2013 period were computed for various return intervals, which is similar to the definition of the trends in this thesis. However, this thesis did not split the data into two distinct periods for the analysis. For the Southeast US, the 1-day 100-yr return period differences in the return values were ~8%

(Wu 2015). This value is ~5% lower than the aggregated Southeast trend estimate from 1890-2011 for the 100-yr return period from the present study, which was ~13%. Wu (2015) did not compute return values for the 2-yr return period. Confidence intervals of the trends were not calculated in Wu (2015) either.

While Sun et al. (2021) found trends in extreme rainfall, the trends are also not quantified, nor are there confidence intervals given, except for intervals connected to extreme precipitation sensitivity to global mean temperatures. This is also the case with Villarini et al. (2012). Villarini et al. (2012) identified the presence of trends, but did not compute the magnitude of those trends, nor the uncertainty through the use of confidence intervals. Wright et al. (2019) also analyzed trends in extreme precipitation using observations. However, the methods for performing the analyses are different from those presented here. For example, Wright et al. (2019) formed clusters of precipitation values that exceeded a certain return value at a given return period rather than on the stations themselves where clusters represented one storm specifically. Furthermore, trends in the clusters were computed through regressions using the El Niño index, the Atlantic Multidecadal Oscillation indices, yearly averaged Northern Hemisphere temperature anomalies, and the Pacific Decadal Oscillation indices as the regression predictors (Wright et al. 2019). Lastly, Wright et al. (2019) also did not compute the confidence intervals of the trends, rather the return periods for the 100-yr daily observed exceedances were found based on the upper bound of the NOAA Atlas 14 confidence intervals.

In comparison, modeling studies have tended to focus on broader extreme precipitation characteristics and trends rather than the magnitude or confidence intervals of such trends. Van der Wiel et al. (2016) is one example of a modeling study that did attempt to quantify trends in extreme precipitation. Trends in precipitation intensity were calculated using the peaks-over-threshold approach, which means that the number of days with precipitation exceeding the rate of a specific event at a given return period were counted. Another difference between van der Wiel et al. (2016) and this thesis comes from how the trends were reported. Here, trends are the percentage change between return values computed for 2020 and 1960, while van der Wiel et al. (2016) reported them as the percent per degree of global warming. Lastly, no statistical distribution was fit to the data prior to the trend analysis (van der Wiel et al. 2016).

Plots generated for the differences in trend estimates between the three datasets used in this study highlight how recent weather events impact extreme precipitation trends. Pooled differences between the full dataset and the dataset truncated at 2011 show that the 2019 trends are larger than those computed in 2011 in regions along the Texas, Louisiana, and South Carolina coasts, which may reflect the influence of storms such as Hurricane Harvey and Hurricane Florence (Fig. 18). Heavier rain producing storms have implications for NOAA Atlas 14. Trends in extreme rainfall imply that the stationary return values calculated in NOAA Atlas 14 may no longer be the best estimates for extreme rainfall risk, particularly for the volumes that were produced several years ago with older data. Updates to volumes such as Volume 2 for North Carolina and South Carolina are likely needed. Pooled trend differences between the full

dataset and 2000 dataset have more spatial variability than those between 2019 and 2011 (Fig. 20). Figure 20 also shows more regions that have larger magnitudes in the trend differences between the datasets. This could be an artifact of additional noise in the data caused by shorter composite station record lengths in the 2000 dataset, which reflects the importance of including more years in trend analyses. Trend differences among the pooled data indicate that the trend estimates are sensitive to various weather events and are therefore unreliable as individual estimates.

Some methods utilized herein to compute the aforementioned trends are unique for extreme precipitation analysis and can be summarized as improving upon previous techniques in various ways. First, precipitation station data were used from 1890 through 2019 to perform the analyses. The extended data record was made possible through the compositing techniques described in Section 2, which allowed for the longer record without decreasing the number of stations that could be used. Other studies used shorter periods of record to account for the lower amount of specific quality observing stations when using individual station time series for the linear trend analysis. This approach leads to larger trend confidence intervals due to an increased margin of error resulting from the smaller sample sizes. Another way in which the present work improves upon previous studies is through the use of the pooling technique. The use of composite stations to form the pooled regions discussed in the results is believed to be unique to this study as it relates to extreme precipitation analysis. The record of block maxima for each station composite within a predefined region was treated as one set of observations prior to fitting the GEV model to it, which refines the trend analysis by decreasing the

noise through the use of more data points. Additionally, this pooling technique allows for the return periods associated with the trends to be acquired, rather than just the trends themselves. Prior studies performed the GEV fit on the individual station time series and then aggregated them, which is challenging to take into account because of the differences between stations' data record quality and length. This approach can also cause trends to be unduly influenced by an individual station's record. Pooling the data prior to fitting the GEV model to the data greatly reduces the impact of individual events and stations. Finally, the use of the global mean surface temperature as the covariate in the nonstationary analysis allows for the extreme rainfall trends to be directly assessed per degree of global warming, which can be beneficial for future adaptation planning as scientists continue to discern how much warming the world will undergo. A nonstationary model using global mean surface temperature as the covariate is also likely a better model of the data. Global temperatures are increasing and do physically affect extreme precipitation, which means that the covariate would fit the data well. Furthermore, global temperature changes are nonlinear. Stationary analyses do not allow the precipitation distribution to change in time and therefore, would act more as a linear fit to the extreme rainfall data. This would lead to higher error variances between the fit and the data, thereby increasing the confidence interval. The nonstationary model with the global mean surface temperature covariate better estimates the present-day risk from extreme rainfall and leads to smaller confidence intervals.

Future work can improve upon and add to the insights gleaned from this study. Although the pooling of regions was done based on the assumption that the composite

counties were all within the same geographical environment for extreme rainfall distributions, this assumption should be examined further to check for statistical consistency. Furthermore, it could be beneficial to determine if better region definitions should be created based on factors such as topography. With additional avenues of examining the data, future work may also involve separating the pooled counties into coastal, near-coastal, and inland regions to compare how the extreme rainfall trends and associated patterns change spatially. One additional analysis that could benefit related studies would be considering the seasonality of these trends, i.e., determining the trend estimates for spring, summer, fall, and winter. Differences in trends between seasons could potentially provide information on where the largest influence in the annual trend is coming from. Finally, more work may be needed to investigate how these trend estimates and the techniques for acquiring them behave across different portions of the US. Specifically, the assumption that stations within counties are interchangeable likely does not work for locations with large topographic relief, which is why this analysis attempted to exclude most counties where that occurs.

REFERENCES

Allen, M. R. and W. J. Ingram, 2002: Constraints on future changes in climate and the hydrologic cycle. *Nat. Insight Review Articles*. **419**, 224-232, doi: 10.1038/nature01092.

Asadieh, B. and N. Y. Krakauer, 2015: Global trends in extreme precipitation: climate models versus observations. *Hydrol. Earth Syst. Sci.,* **19**, 877-891, doi: 10.5194/hess-19-877-2015.

Bonnin, G. M., D. Martin, B. Lin, T. Parzybok, M. Yekta, and D. Riley, 2006: NOAA Atlas 14: Precipitation-Frequency Atlas of the United States, Volume 2 Version 3.0, NOAA, National Weather Service, Silver Spring, Maryland.

Brown, V. M., B. D. Keim, and A. W. Black, 2020: Trend Analysis of Multiple Extreme Hourly Precipitation Time Series in the Southeastern United States. *J. Appl. Meteor. Climatol.* **59**, 427-442, doi: 10.1175/jamc-d-19-0119.1.

Chao, L., F. Zwiers, X. Zhang, G. Li, Y. Sun, and M. Wehner, 2021: Changes in annual extremes of daily temperature and precipitation in CMIP6 models. *J. Climate*, **34**, 3441-3460, doi: 10.1175/JCLI-D-19-1013.1.

Dai, A., 2006: Precipitation characteristics in eighteen coupled climate models. *J. Climate*, **19**, 4605-4630.

El Adlouni, S., T. B. M. J. Ouarda, X. Zhang, R. Roy, and B. Bobée, 2007: Generalized maximum likelihood estimators for the nonstationary generalized extreme value model, *Water Resour. Res.*, **43**, W03410, doi:10.1029/2005WR004545.

Feng, X., C. Liu, F. Xie, J. Lu, L. S. Chiu, G. Tintera, and B. Chen, 2019: Precipitation characteristic changes due to global warming in a high-resolution (16 km)

ECMWF simulation. *Quart. J. Roy. Meteor. Soc.*, **145**, 303-317, doi: https://doi.org/10.1002/qj.3432.

Fischer, E. M., and R. Knutti, 2016: Observed heavy precipitation increase confirms theory and early models. *Nat. Clim. Change*, **6**, 986-991, doi: 10.1038/nclimate3110.

Giorgi, F., F. Faffaele, and E. Coppola, 2019: The response of precipitation characteristics to global warming from climate projections. *Earth Syst. Dynam.*, **10**, 73-89, doi: 10.5194/esd-10-73-2019.

Held, I. M. and B. J. Soden, 2006: Robust responses of the hydrological cycle to global warming. *J. Climate*, **19**, 5686-5699.

Hershfield, D.M., 1961: Technical Paper No. 40: Rainfall frequency atlas of the United States for durations from 30 minutes to 24 hours and return periods from 1 to 100 years, 65.

Janssen, E., D. J. Wuebbles, K. E. Kunkel, S. C. Olsen, and A. Goodman, 2014: Observational- and model-based trends and projections of extreme precipitation over the contiguous United States. *Earth's Future*, **2**, 99-113, doi: 10.1002/2013EF000185.

Knutti, R., and J. Sedlacek, 2012: Robustness and uncertainties in the new CMIP5 climate model projections. *Nat. Clim. Change*, **3**, 369-373, doi: 10.1038/nclimate1716.

Kunkel, K. E., and S. M. Champion, 2019: An Assessment of Rainfall from Hurricanes Harvey and Florence Relative to Other Extremely Wet Storms in the United States. *Geophys. Res. Lett.*, **46,** 13500-13506, doi: 10.1029/2019gl085034.

Kunkel, K. E. and Coauthors, 2013: Monitoring and Understanding Trends in Extreme Storms: State of Knowledge. *Bull. Amer. Meteor. Soc.*, **94**, 499-514, doi: 10.1175/bams-d-11-00262.1.

Kunkel, K. E., T. R. Karl, M. F. Squires, X. Yin, S. T. Stegall, and D. R. Easterling, 2020: Precipitation Extremes: Trends and Relationships with Average Precipitation and Precipitable Water in the Contiguous United States. *J. Appl. Meteor. Climatol.* **59**, 125-142, doi: 10.1175/jamc-d-19-0185.1.

Martel, J., A. Mailhot, F. Brissette, and D. Caya, 2018: Role of natural climate variability in the detection of anthropogenic climate change signal for mean and extreme precipitation at local and regional scales. *J. Climate*, **31**, 4241-4263, doi: 10.1175/JCLI-D-17-0282.1.

Martins, E. S., and J. R. Stedinger, 2000: Generalized maximum-likelihood generalized extreme-value quantile estimators for hydrologic data. *Water Resour. Res.*, **36(3)**, 737–744, doi: 10.1029/1999WR900330.

Mascioli, N. R., A. M. Fiore, M. Previdi, and G. Correa, 2016: Temperature and Precipitation Extremes in the United States: Quantifying the Responses to Anthropogenic Aerosols and Greenhouse Gases. *J. Climate*, **29**, 2689-2701, doi: 10.1175/jcli-d-15-0478.1.

Mehran, A., A. AghaKouchak, and T. J. Phillips, 2014: Evaluation of CMIP5 continental precipitation simulations relative to satellite-based gauge-adjusted observations. *J. Geophys. Res. Atmos*., **119**, 1695-1707, doi: 10.1002/2013JD021152.

Meinshausen, M., S. Smith, et al., 2011: "The RCP Greenhouse Gas Concentrations and their extension from 1765 to 2500", Climatic Change (Special Issue on RCPs), accessed 14 September 2021, http://www.pik-potsdam.de/~mmalte/rcps/.

Menne, M.J., I. Durre, R.S. Vose, B.E. Gleason, and T.G. Houston, 2012: An overview of the Global Historical Climatology Network-Daily database. *J. Atmos. Oceanic. Technol.*, **29**, 897-910, doi: 10.1175/JTEH-D-11-00103.1.

Myhre, G., E. J. Highwood, K. P. Shine, and F. Stordal, 1998: New estimates of radiative forcing due to well mixed greenhouse gases. *Geophys. Res. Lett.*, **25**, 2715-2718, doi: 10.1029/98gl01908.

Paciorek, C.J., D.A. Stone, and M.F. Wehner, 2018: Quantifying statistical uncertainty in the attribution of human influence on severe weather. *Wea. Clim. Extremes*, **20**, 69-80, doi: 10.1016/j.wace.2018.01.002.

Pendergrass, A. G., and D. L. Hartmann, 2014: Changes in the Distribution of Rain Frequency and Intensity in Response to Global Warming. *J. Climate*, **27**, 8372-8383, doi: 10.1175/jcli-d-14-00183.1.

Perica, S., D. Martin, S. Pavlovic, I. Roy, M. St. Laurent, C. Trypaluk, D. Unruh, M. Yekta, and G. Bonnin, 2013: NOAA Atlas 14: Precipitation-Frequency Atlas of the United States, Volume 9 Version 2: Southeastern States. NOAA, National Weather Service, Silver Spring, MD.

Perica, S., S. Pavlovic, M. St. Laurent, C. Trypaluk, D. Unruh, O. Wilhite, 2018: NOAA Atlas 14: Precipitation-Frequency Atlas of the United States, Volume 11 Version 2.0: Texas. NOAA, National Weather Service, Silvers Spring, Maryland.

Pfahl, S., P. A. O'Gorman, and E. M. Fischer, 2017: Understanding the regional pattern of projected future changes in extreme precipitation. *Nat. Clim. Change*, **7**, 423-428, doi: 10.1038/nclimate3287.

Prein, A. F., C. Liu, K. Ikeda, S. B. Trier, R. M. Rasmussen, G. J. Holland, and M. P. Clark, 2017: Increased rainfall volume from future convective storms in the US. *Nat. Clim. Change*, **7**, 880-884, doi: https://doi.org/10.1038/s41558-017-0007-7.

Risser, M.D., and M.F. Wehner, 2017: Attributable human-induced changes in the likelihood and magnitude of the observed extreme precipitation during Hurricane Harvey. *Geophys. Res. Lett.*, **44**, 12457-12464, doi: 10.1002/2017GL075888.

Sun, Q., X. Zhang, F. Zwiers, S. Westra, and L. V. Alexander, 2021: A global, continental, and regional analysis of changes in extreme precipitation. *J. Climate*, **34**, 243-258, doi: 10.1175/JCLI-D-19-0892.1.

Trenberth, K. E., 2011: Changes in precipitation with climate change. *Climate Res.*, **47**, 123-138, doi: 10.3354/cr00953.

van der Wiel, K., and Coauthors, 2016: The Resolution Dependence of Contiguous U.S. Precipitation Extremes in Response to CO2 Forcing. *J. Climate*, **29**, 7991-8012, doi: 10.1175/jcli-d-16-0307.1.

Villarini, G., J. A. Smith, and G. A. Vecchi, 2013: Changing frequency of heavy rainfall over the central United States. *J. Climate*, **26**, 351-357, doi: 10.1175/JCLI-D-12-00043.1.

Vu, T. M., and A. K. Mishra, 2019: Nonstationary frequency analysis of the recent extreme precipitation events in the United States. *J. Hydrol.*, **575**, 999-1010, doi: https://doi.org/10.1016/j.jhydrol.2019.05.090.

Wehner, M., P. Gleckler, and J. Lee, 2020: Characterization of long period return values of extreme daily temperature and precipitation in the CMIP6 models: Part 1, model evaluation. *Wea. Climate Extremes*, **30**, 1-15, doi: https://doi.org/10.1016/j.wace.2020.100283.

Westra, S., and Coauthors, 2014: Future changes to the intensity and frequency of short-duration extreme rainfall. *Rev. Geophys.*, **52**, 522-555, doi: 10.1002/2014rg000464.

Wright, D. B., C. D. Bosma, and T. Lopez-Cantu, 2019: U.S. Hydrologic Design Standards Insufficient Due to Large Increases in Frequency of Rainfall Extremes. *Geophys. Res. Lett.*, **46**, 8144-8153, doi: 10.1029/2019gl083235.

Wu, S., 2015: Changing characteristics of precipitation for the contiguous United States. *Climate Change*, **132**, 677-692, doi: 10.1007/s10584-015-1453-8.